TOR VERGATA
UNIVERSITÀ DEGLI STUDI DI ROMA

Towards Digital Twin Technologies for Ascending Aortic Aneurysm Growth Prediction and Real-Time Diagnosis

Supervisor: Prof. Pier Paolo Valentini

Candidate: Leonardo Geronzi

Co-Supervisor: Prof. Marco Evangelos Biancolini

Co-Supervisor: PhD Michel Rochette

Coordinator: Prof. Francesco Vivio

December 1st, 2023

PhD Cycle: 36
Academic Year: 2023/2024

Department of Enterprise Engineering "Mario Lucertini"

My MeDiTATe PhD journey

MEDITATE

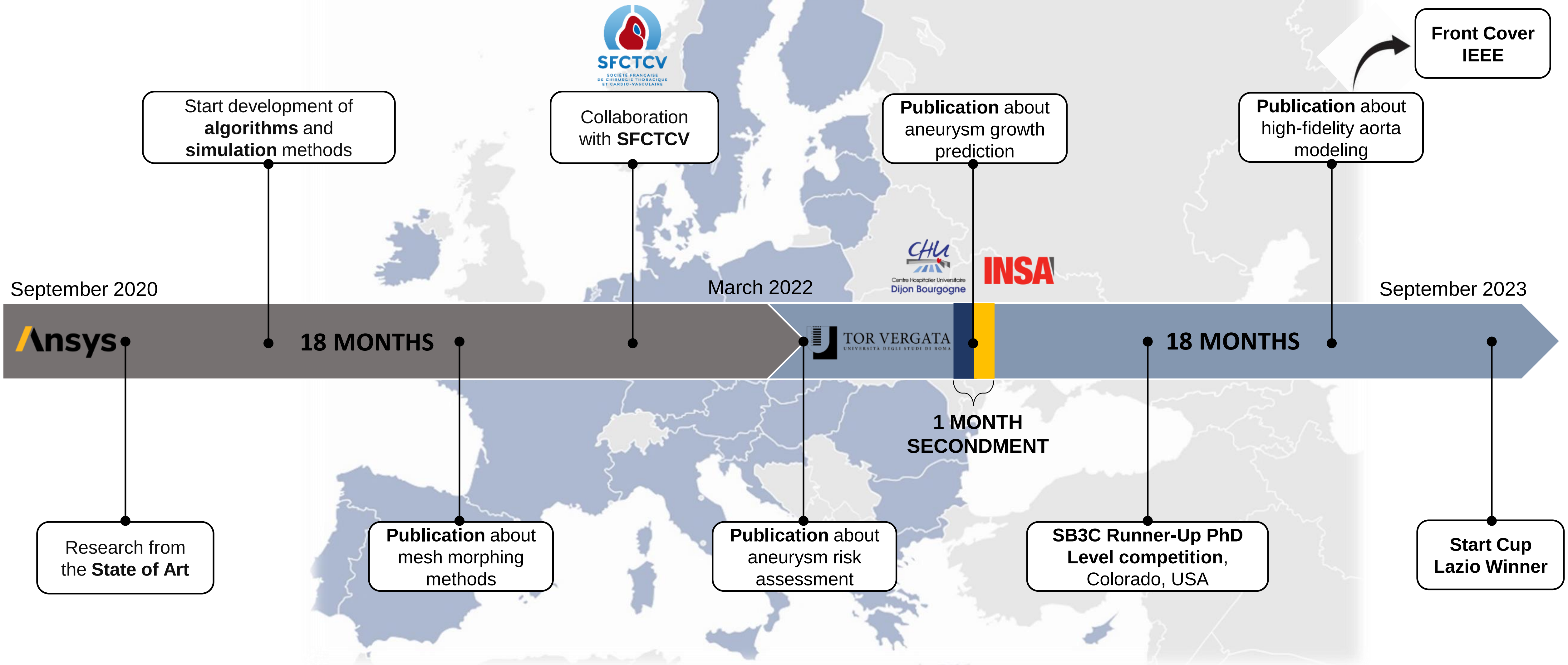

Overview

INTRODUCTION

- The clinical problem
- The clinical challenges
- The computational context
- The computational challenges
- The Digital Twin
- Purpose of the work

MATERIALS & METHODS AND RESULTS

- **PART 1** Shape-based ascending aortic aneurysm growth prediction
- **PART 2** High-fidelity aorta modeling accounting for the heart motion and the interaction with the surrounding tissues
- **PART 3** Hemodynamic real-time prediction based on surrogate modeling techniques

CONCLUSIONS

LIST OF PUBLICATIONS

The clinical problem

The heart and the main vessels

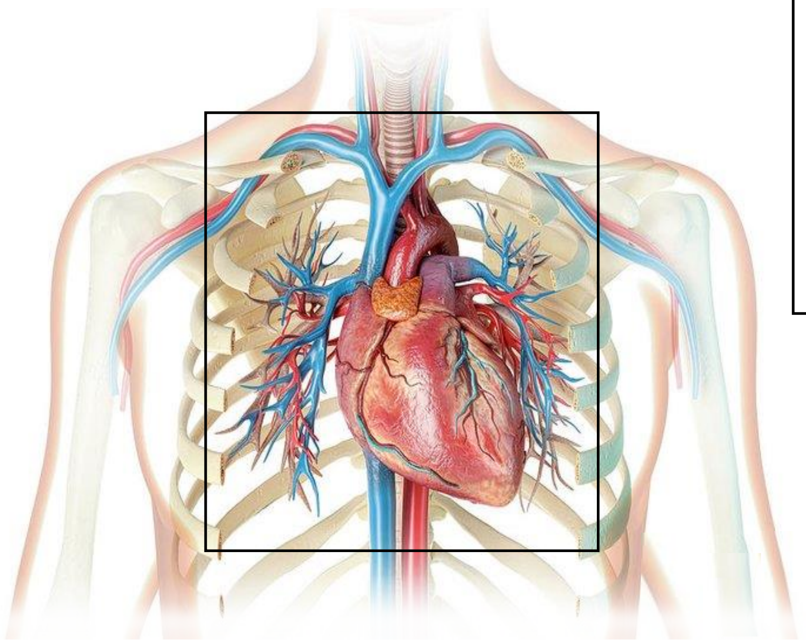

The thoracic aorta (TA)

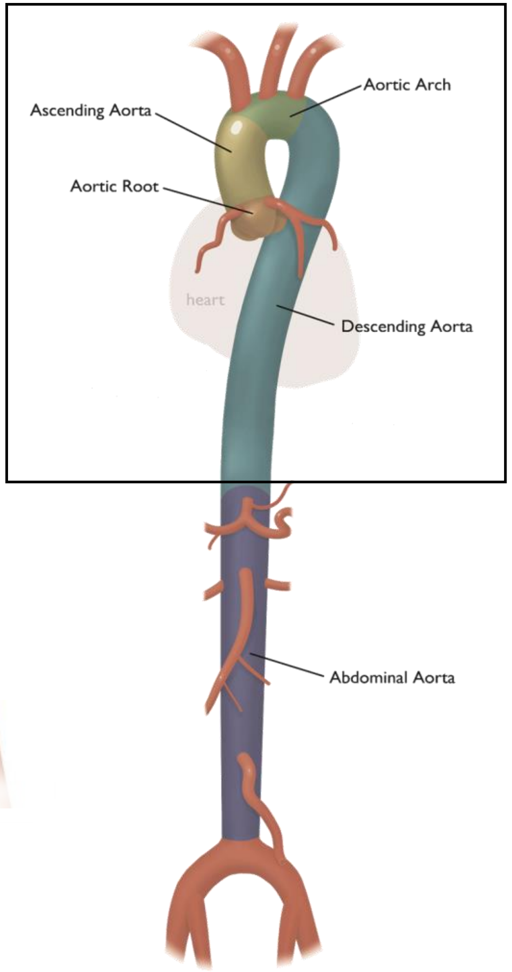

The ascending aortic aneurysm (AsAA)

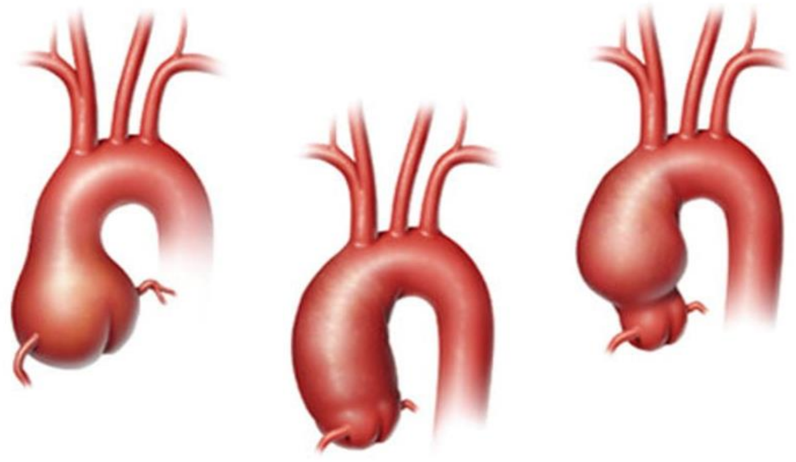

PREVALENCE [1]

$5.3 \text{ per } \frac{100\,000}{year}$

INCIDENCE [1]

0.16% population

[1] E Melo, et al., Seminars in thoracic and cardiovascular surgery, Vol. 34, No. 1, pp. 1-16, 2022.

The clinical challenges

Diameter (D): main criterion to access **surgery**

Surgery is highly **invasive** and carries intra and post-operative risks for the patient

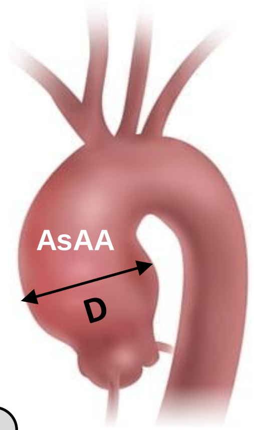

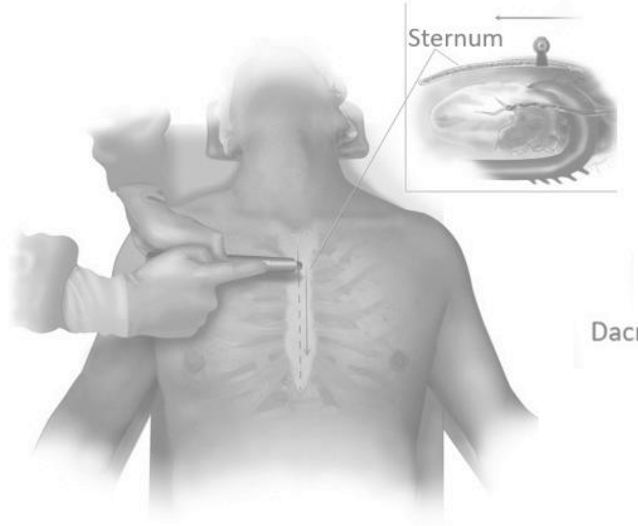

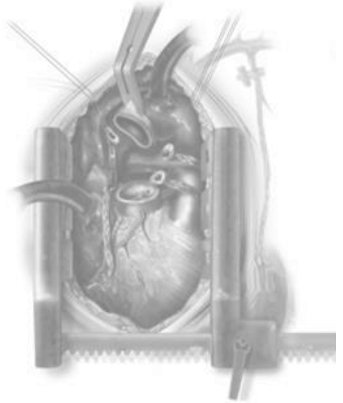

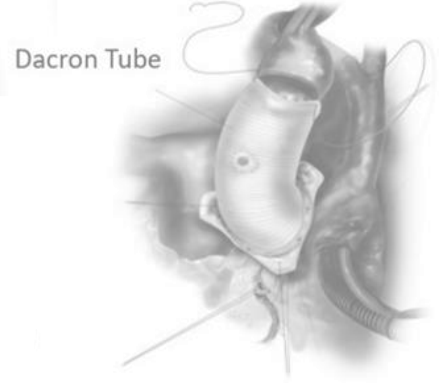

The challenges related to the AsAA

The "**small aorta**" [2] problem

Surgical **timing** is crucial for optimal patient outcomes [3]

A careful and comprehensive **risk assessment** is necessary

[2] **Elective replacement of the ascending aorta: is the 5.5-cm threshold appropriate? The insidious, small aorta**
Nikolaos A. Papakonstantinou [a,*] and Filippos-Paschalis Rorris [b]
European Journal of Cardio-Thoracic Surgery 59 (2021) 554–561

[3] **Natural history and risk factors for rupture of thoracic aortic arch aneurysms**
Rachel S. Yiu MBBS, Stephen W.K. Cheng MBBS, MS, FRCS
Journal of Vascular Surgery
Volume 63, Issue 5, May 2016, Pages 1189-1194

The computational context

1 Imaging techniques

- Ultrasounds (US) techniques
- Computed tomography (CT)
- Magnetic resonance imaging (MRI)

→ Morphological and functional data

2 Material characterization

→ Tissue properties

3 Computational modeling

Computer Aided Engineering (CAE) can be used for performing **patient-specific** analysis

- Biomechanical behaviour → Computational Solid Mechanics (CSM)
- Hemodynamic condition → Computational Fluid Dynamics (CFD)

CSM + CFD → Fluid-Structure Interaction (FSI)

The computational challenges

Numerical simulation requirements

Accuracy

The simulation must precisely model complex biological and physical processes.

PROBLEM

Data availability and data **integration**

Robustness

The simulation should reproduce several scenarios and variables, ensuring consistent performance across different conditions.

PROBLEM

Deep technical **expertise** at every step of the model creation

Efficiency

The simulation should deliver results in a time frame compatible with its purpose.

PROBLEM

High **computational costs** and **resources**

The Digital Twin

A **Digital Twin** [4] is a virtual representations of physical objects, systems or processes updated through the exchange of information between the real and virtual domains

1. **Life-cycle follow-up (future state prediction)**
2. **High accuracy and fidelity**
3. **(Quasi) real-time reaction**
4. **Interconnectivity**

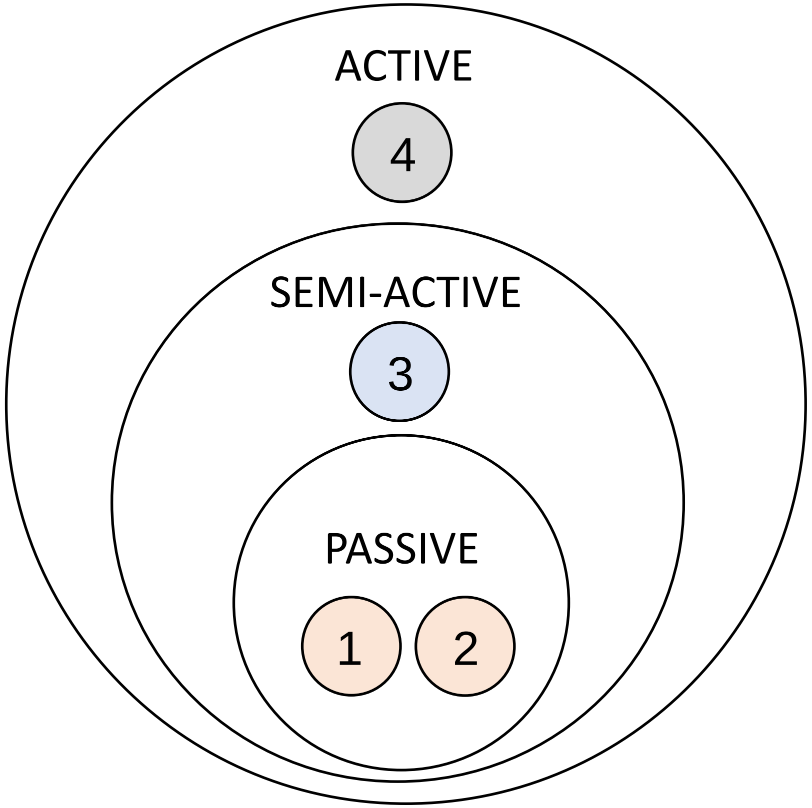

Digital Twins in cardiovascular care can **help the clinicians** in performing **diagnosis** of aortic diseases, **personalized treatment planning** and in monitoring the aneurysm progression.

[4] VanDerHorn et al., "Digital Twin: Generalization, characterization and implementation." Decision support systems 145 (2021): 113524.

Purpose of the work

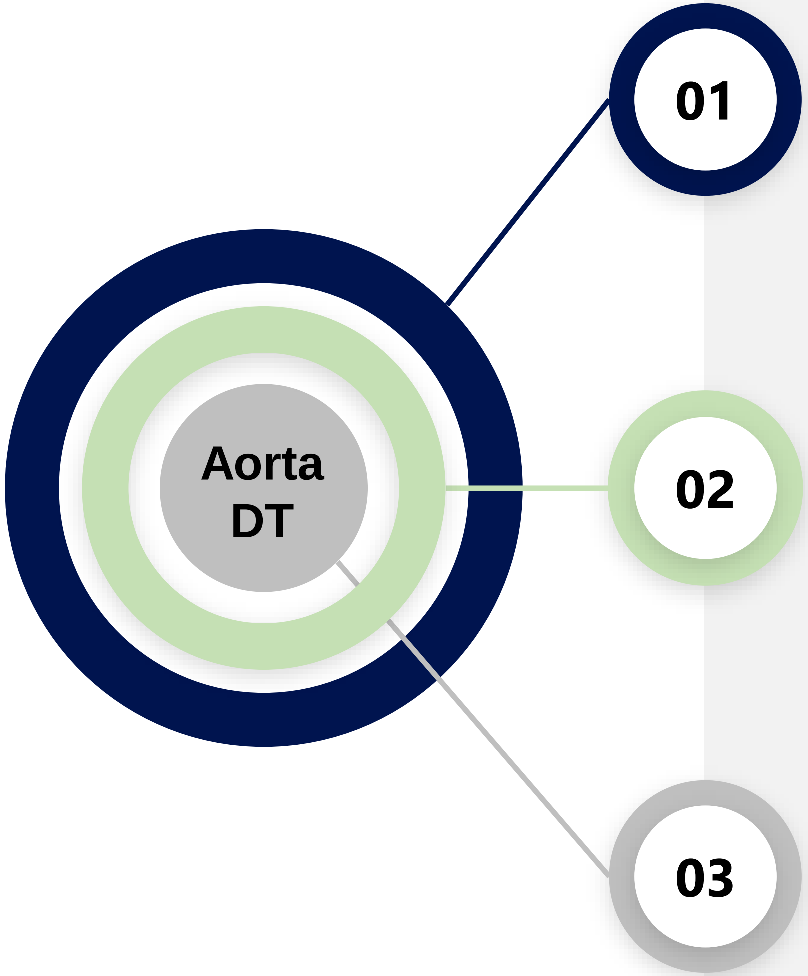

PART 1

Redefining risk prediction metrics based on the aortic anatomy

- Move beyond the maximum diameter criterion.
- Develop growth predictors for a Digital Twin to estimate future conditions.

PART 2

Implementing high-fidelity thoracic aorta models

- Replicate the real aorta kinematics for the effective study of the wall behaviour.
- Integrate patient-specific properties.

PART 3

Developing a procedure for real-time hemodynamic assessment

- Deliver surrogate models for instantaneous Digital Twin responses.
- Facilitate rapid transition from medical images to simulation results.

PART 1

SHAPE-BASED ASCENDING AORTIC ANEURYSM GROWTH PREDICTION

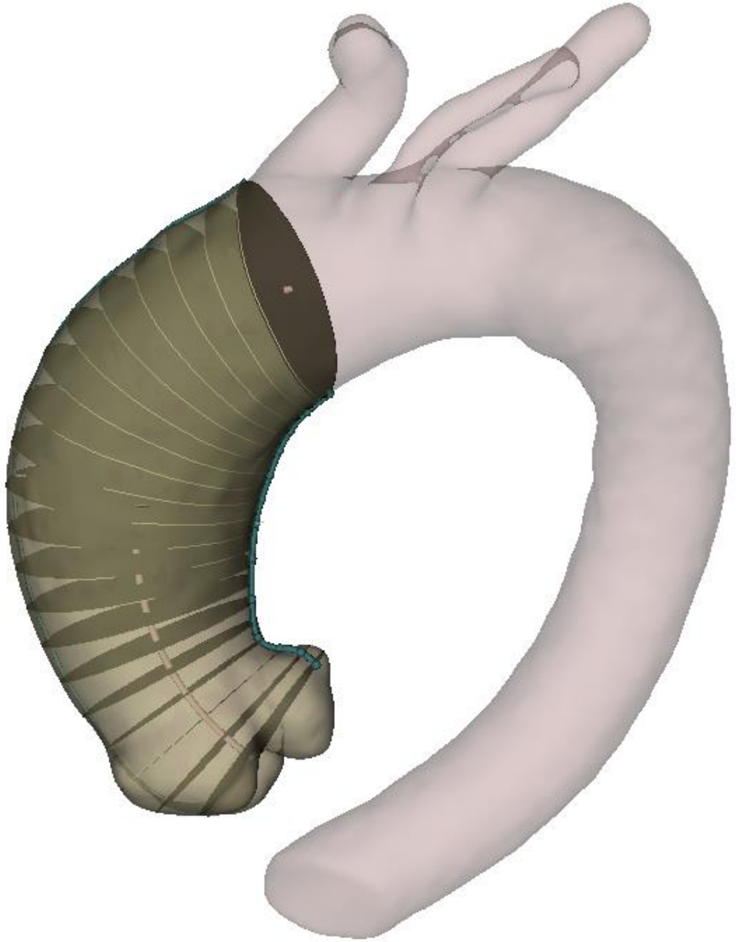

The ascending aorta dataset

LONGITUDINAL DATA

CT-Scan and 3D MRI

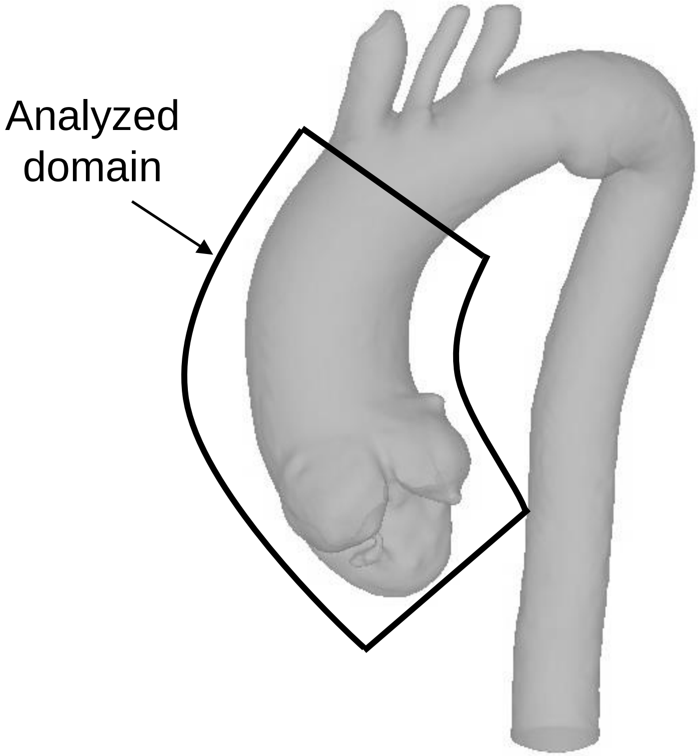

EXCLUSION CRITERIA

70
PATIENTS

- Less than 6 months between the exams
- Age $\leq$ 25 years old
- Infection, systemic inflammatory, dissection
- Congenital tissue disorder (Marfan)
- Images with artefacts
- Prior valvular surgery

Local shape features

$$\Delta Diameter = D_{MAX_{time\ 2}} - D_{MAX_{time\ 1}}$$

$$\Delta time = Time\ 2 - Time\ 1$$

DIAMETER ALONG THE CENTERLINE

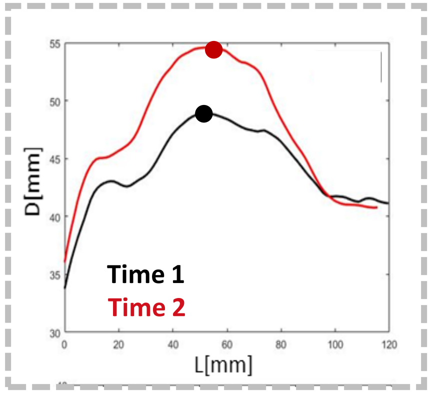

ASSUMPTION OF LINEAR GROWTH

$$Growth\ Rate\ (GR) = \frac{\Delta Diameter}{\Delta time}$$

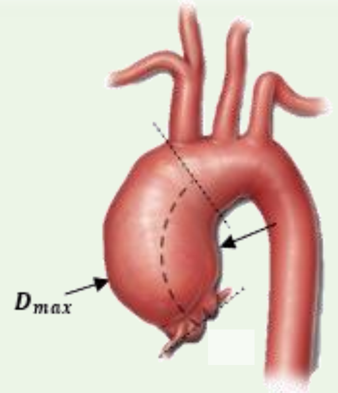

$(1)\ D_{max}$

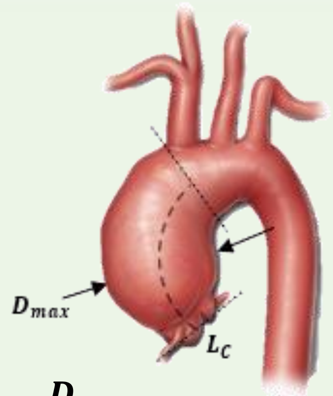

$(2)\ DCR = \frac{D_{max}}{L_C}$

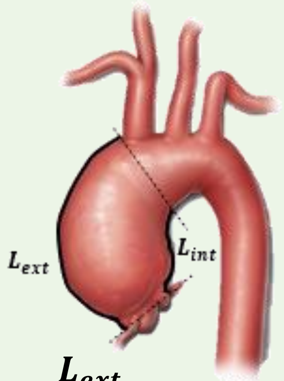

$(3)\ EILR = \frac{L_{ext}}{L_{int}}$

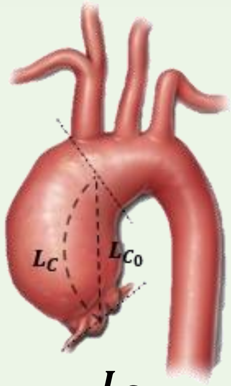

$(4)\ T = \frac{L_C}{L_{C_0}}$

Correlation between aneurysm **GR** and **local shape features** is first sought.

Machine learning (ML) based risk prediction

DATABASE (70 patients)

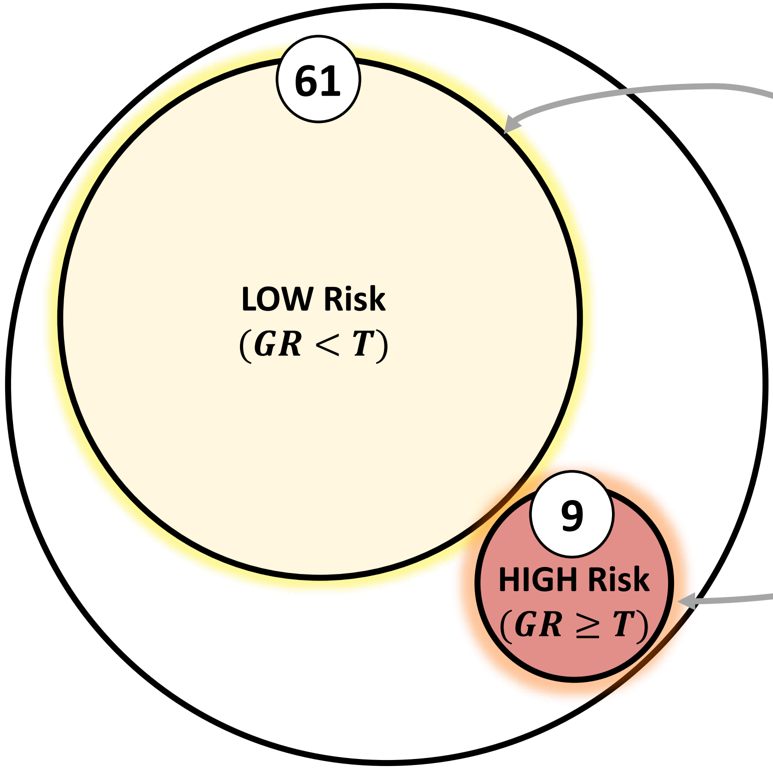

Growth rate threshold
T=0.25 mm/month

6 ML classifiers are trained using local shape features to predict which class the patient belongs to.

D | D+DCR+EILR+T

1. Decision Tree (DT)
2. Linear Discriminant (LD)
3. Logistic Regression (LR)
4. Naive Bayes (NB)
5. Support Vector Machine (SVM)
6. K-Nearest Neighbours (KNN)

Leave-one-out procedure

$$Accuracy = \frac{TP + TN}{TP + TN + FP + FN}$$

$$Sensitivity = \frac{TP}{TP + FN}$$

$$Specificity = \frac{TN}{TN + FP}$$

$$LHR_+ = \frac{Sensitivity}{1 - Specificity}$$

$$LHR_- = \frac{1 - Sensitivity}{Specificity}$$

Global shape features

- Extracted from the **entire** population.
- Based on the full ascending aorta **computational grids** derived using mesh morphing.

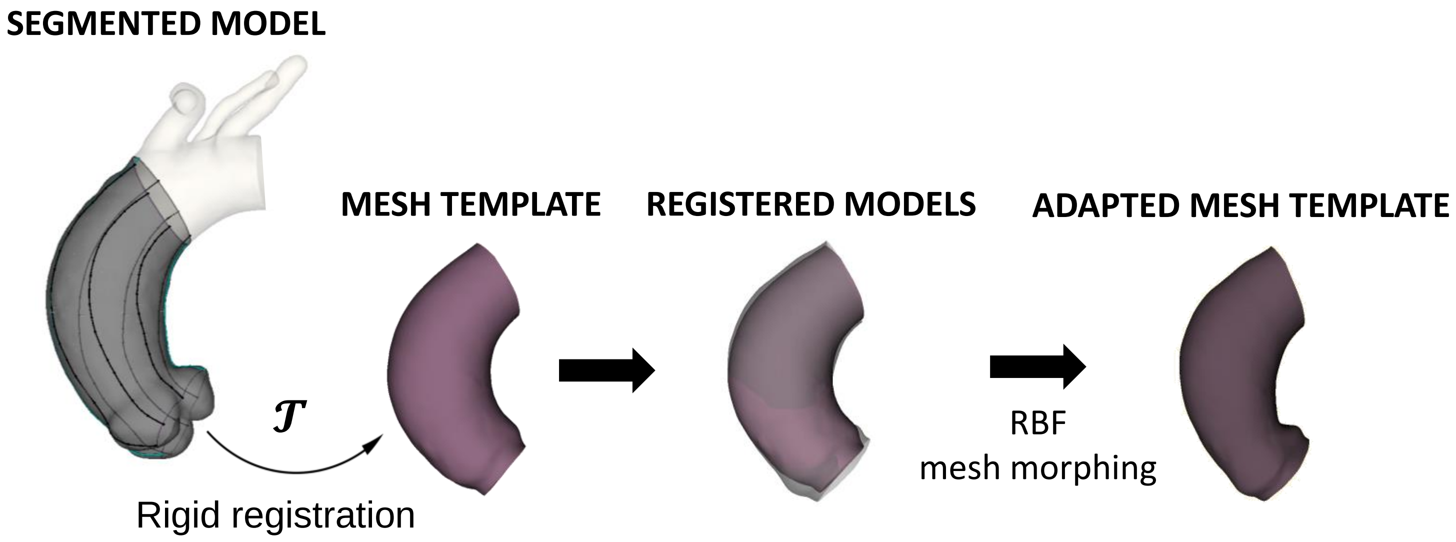

Global shape features

- Extracted from the **entire** population.
- Based on the full ascending aorta **computational grids** derived using mesh morphing.

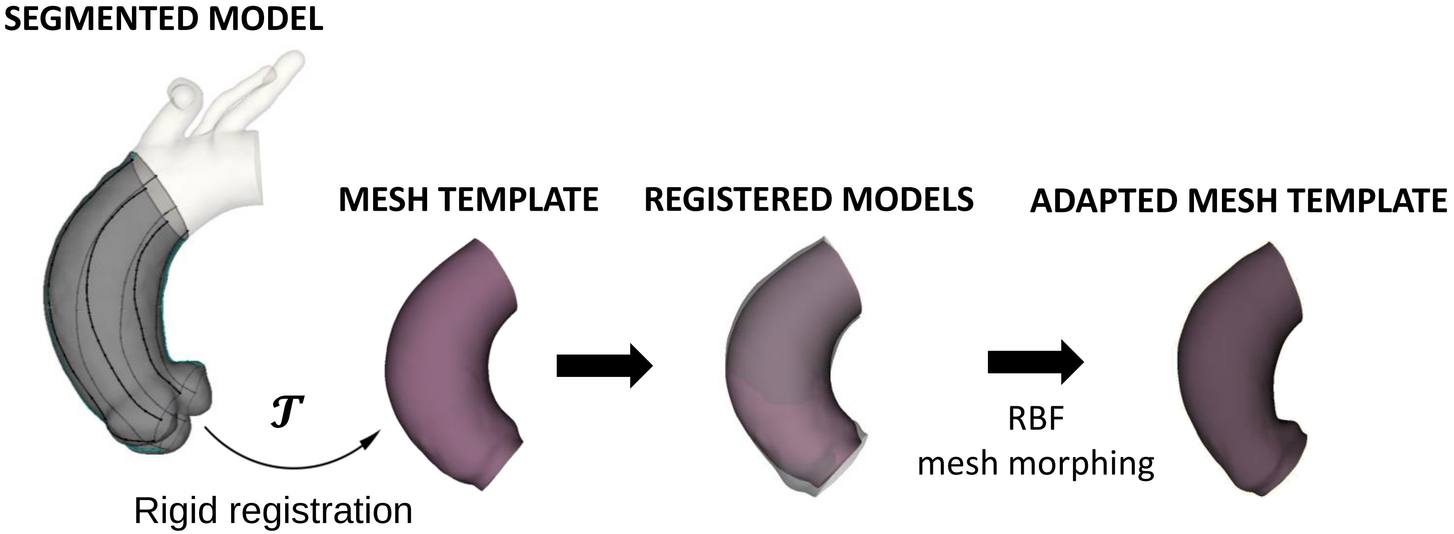

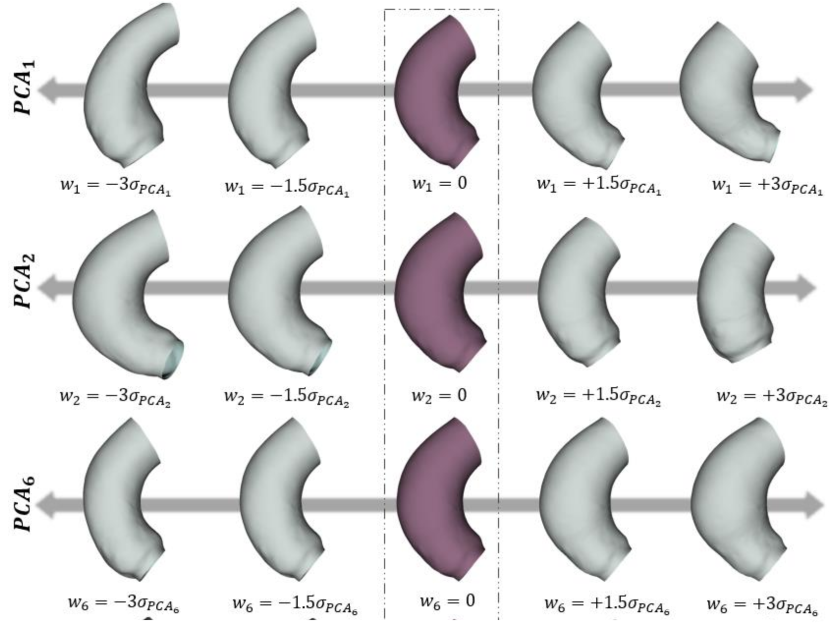

Statistical shape analysis

$$\tilde{\boldsymbol{x}}(\boldsymbol{w}) = \overline{\boldsymbol{x}} + \boldsymbol{\phi}\boldsymbol{w}_{\boldsymbol{x}}$$

$$\boldsymbol{w}_{\boldsymbol{x}} = \boldsymbol{\phi}^{\boldsymbol{T}}(\boldsymbol{x} - \overline{\boldsymbol{x}})$$

$$-3\sqrt{\lambda_i} \leq w_i \leq 3\sqrt{\lambda_i}$$

Dimensionality reduction method

Principal component analysis (PCA)

Global shape features

- Extracted from the **entire** population.
- Based on the full ascending aorta **computational grids** derived using mesh morphing.

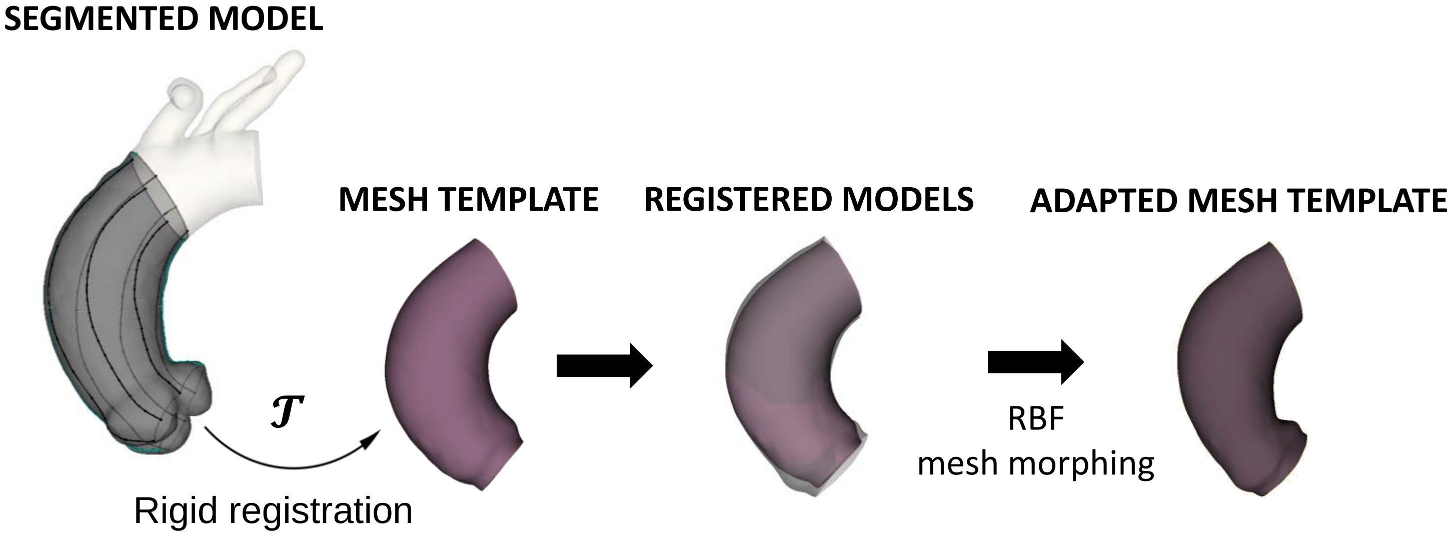

Statistical shape analysis

$$\tilde{x}(w) = \bar{x} + \phi w_x$$
$$w_x = \phi^T(x - \bar{x})$$
$$-3\sqrt{\lambda_i} \leq w_i \leq 3\sqrt{\lambda_i}$$

Dimensionality reduction method

Principal component analysis (PCA)

Partial least squares (PLS)

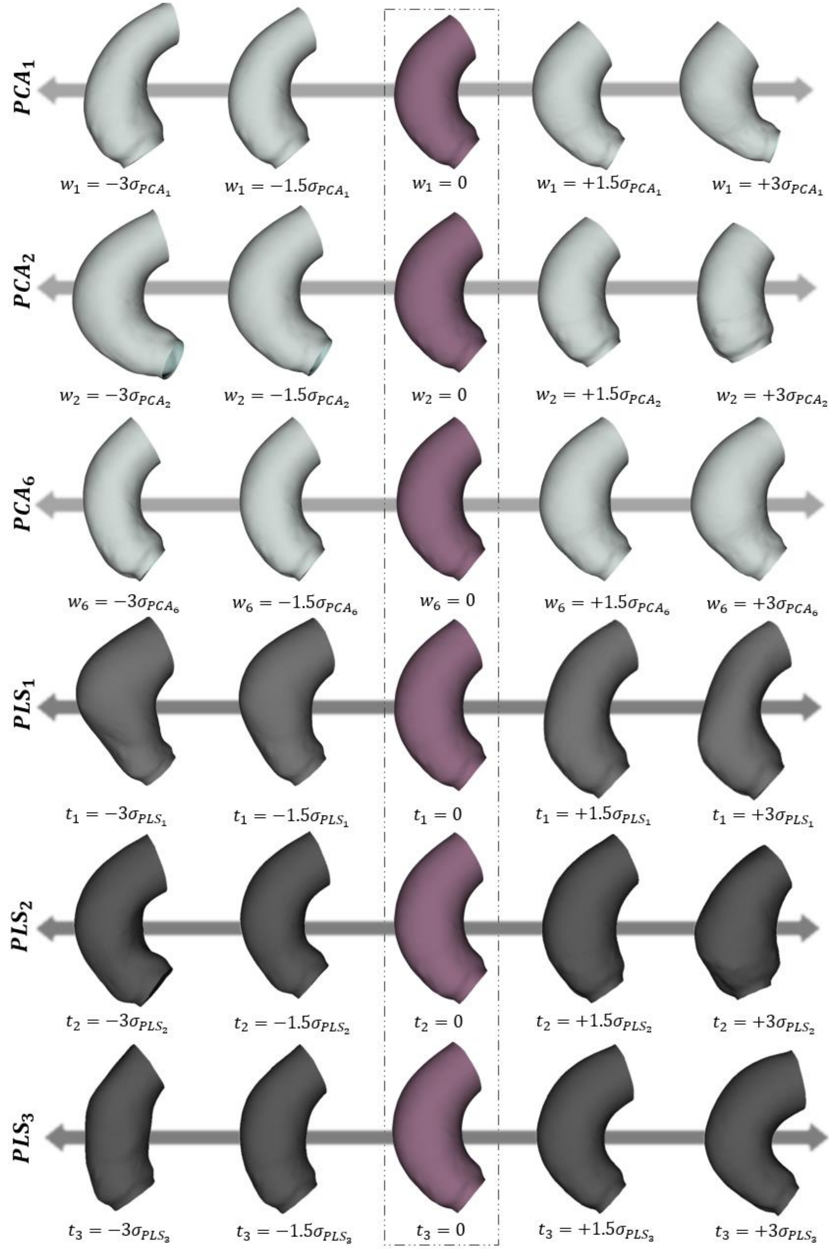

Regression methods

- Extracted fro
- Based on the

SEGMENTED MODE

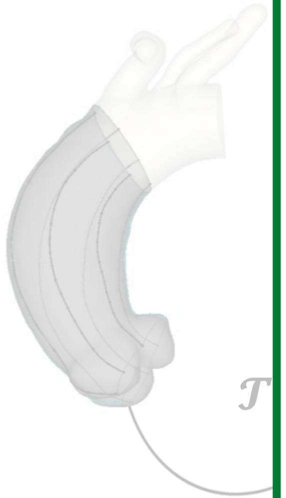

Rigid registration

Statistical

$$\tilde{x}(w) = \bar{x} + \phi w_x$$
$$w_x = \phi^T(x - \bar{x})$$
$$-3\sqrt{\lambda_i} \le w_j \le 3\sqrt{\lambda_i}$$

Regression methods to **directly infer** the growth rate (**GR**)

LOCAL SHAPE FEATURES

DCR, EILR, T

GLOBAL SHAPE FEATURES

PCA-derived

PLS-derived

SVM regression Gaussian kernel function (local shape features, PCA-derived)

Linear regression (PLS-derived)

RESULTS: R^2, $RMSE$

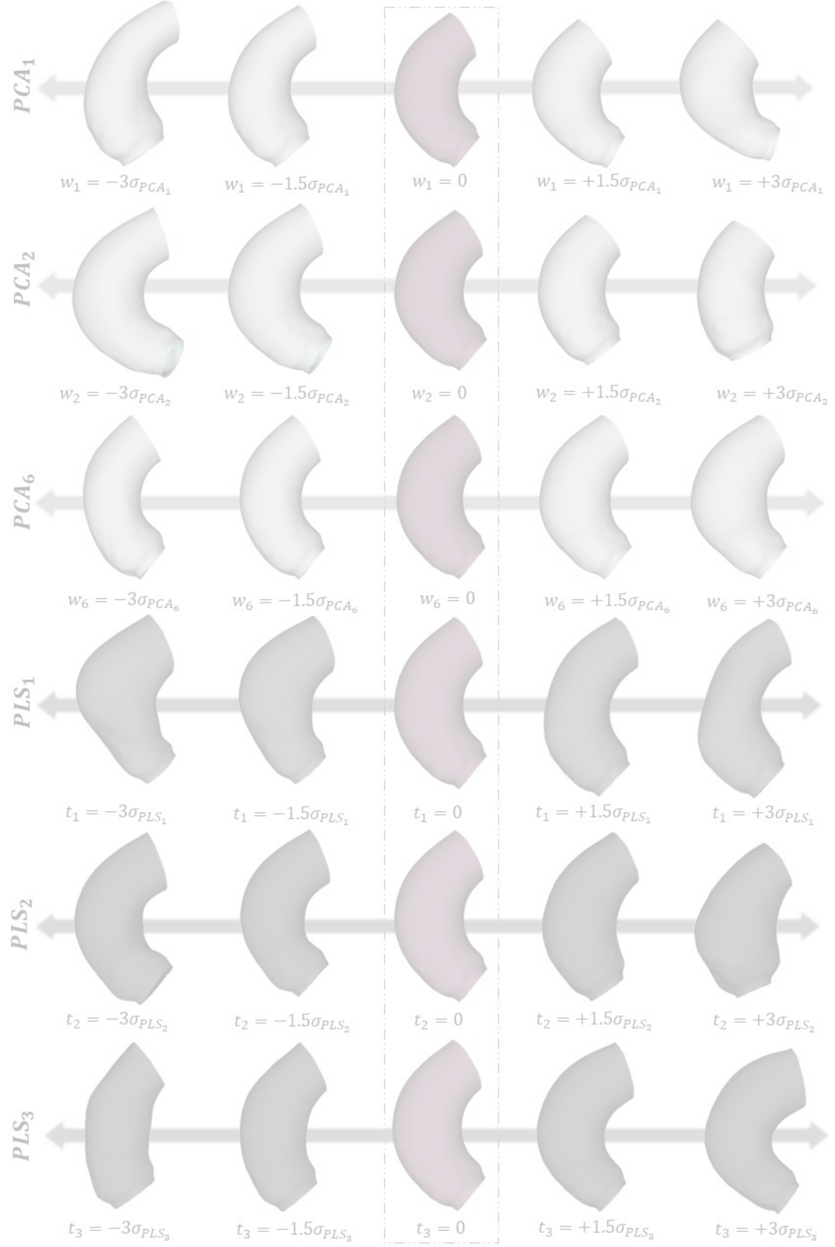

Correlation local shape features and growth rate

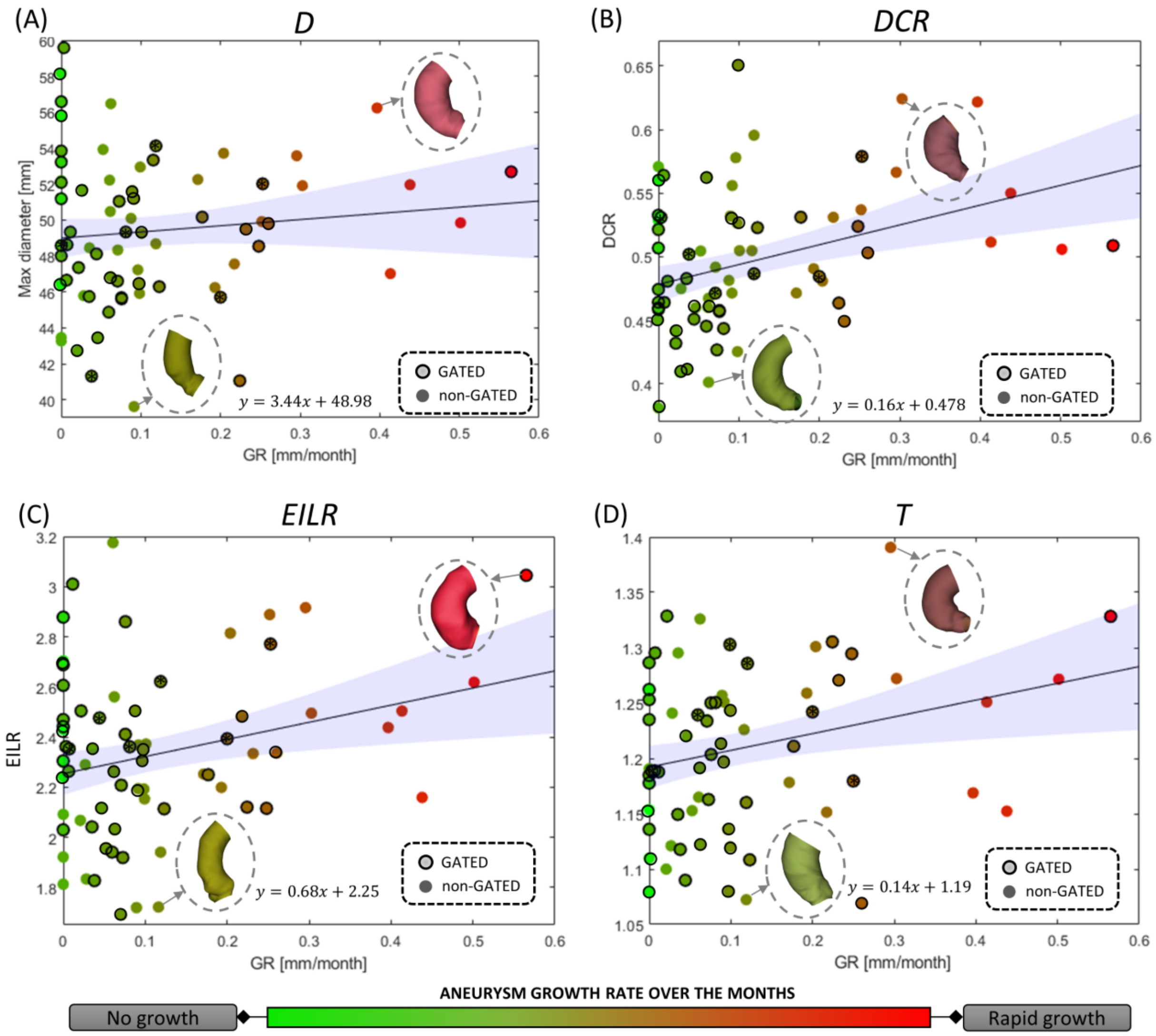

Parameters

	Median value	Interquartile range
D	49,29 mm	5,72 mm
DCR	0.48	0.07
EILR	2.32	0.39
T	1.22	0.11
GR	0.08 mm/month	0.17 mm/month

Spearman's coefficients

	R value	p-value
D	0,087	0,237
DCR	0,478	1.4e-5
EILR	0.411	2e-4
T	0.241	0.02

Growth risk prediction

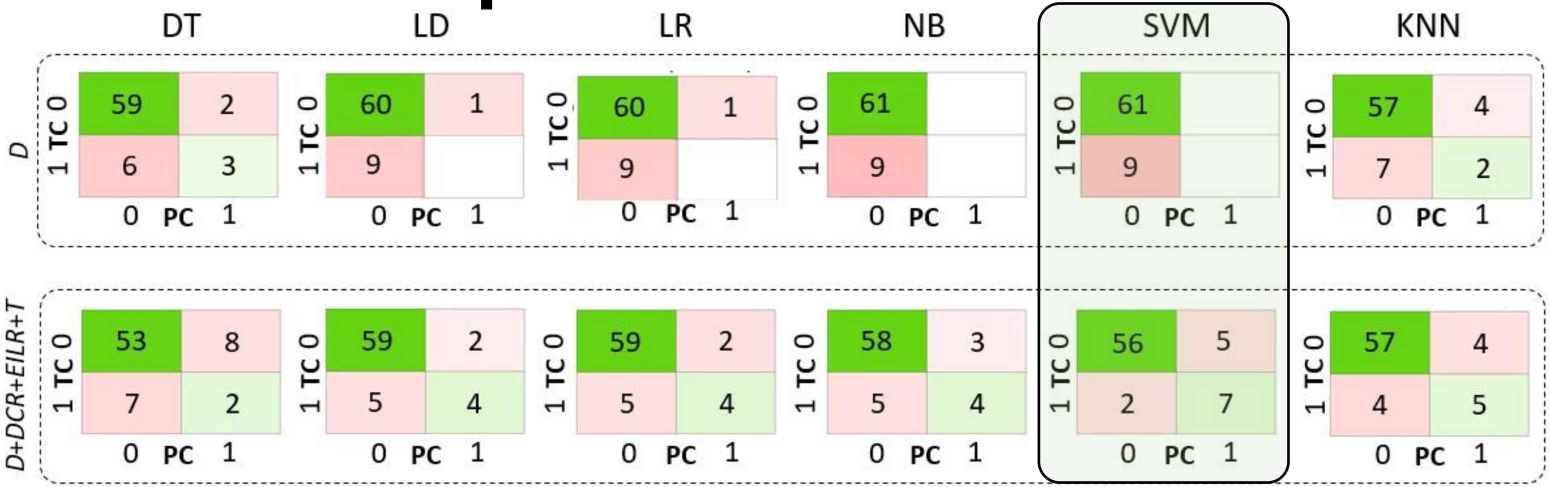

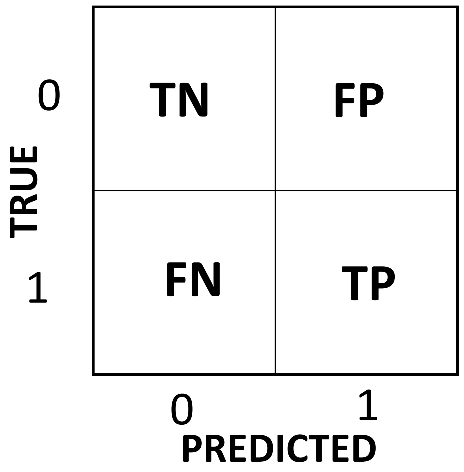

	DT	LD	LR	NB	SVM	KNN
Accuracy (*D*)	**88.6%**	85.7%	85.7%	87.1%	87.1%	84.3%
Accuracy (*D+DCR+EILR+T*)	78.8%	**90%**	**90%**	88.6%	**90%**	88.6%
Sensitivity (*D*)	**33.3%**	0%	0%	0%	0%	22.2%
Sensitivity (*D+DCR+EILR+T*)	22.2%	44.4%	44.4%	44.4%	**77.8%**	55.6%
Specificity (*D*)	96.7%	98.4%	98.4%	**100%**	**100%**	93.4%
Specificity (*D+DCR+EILR+T*)	86.9%	**96.7%**	**96.7%**	95.1%	91.8%	93.4%
LHR+ (*D*)	**10.1**	0	0	//	//	3.36
LHR+ (*D+DCR+EILR+T*)	1.7	**13.5**	**13.5**	9.1	9.5	8.4
LHR- (*D*)	**0.69**	1.02	1.02	1	1	0.83
LHR- (*D+DCR+EILR+T*)	0.89	0.57	0.57	0.58	**0.24**	0.48

$$Accuracy = \frac{TP + TN}{TP + TN + FP + FN}$$

$$Sensitivity = \frac{TP}{TP + FN} \qquad Specificity = \frac{TN}{TN + FP}$$

$$LHR_{+} = \frac{Sensitivity}{1 - Specificity} \qquad LHR_{-} = \frac{1 - Sensitivity}{Specificity}$$

Growth rate prediction: local versus global shape features

Local shape features (*DCR* + *EILR* +*T*)

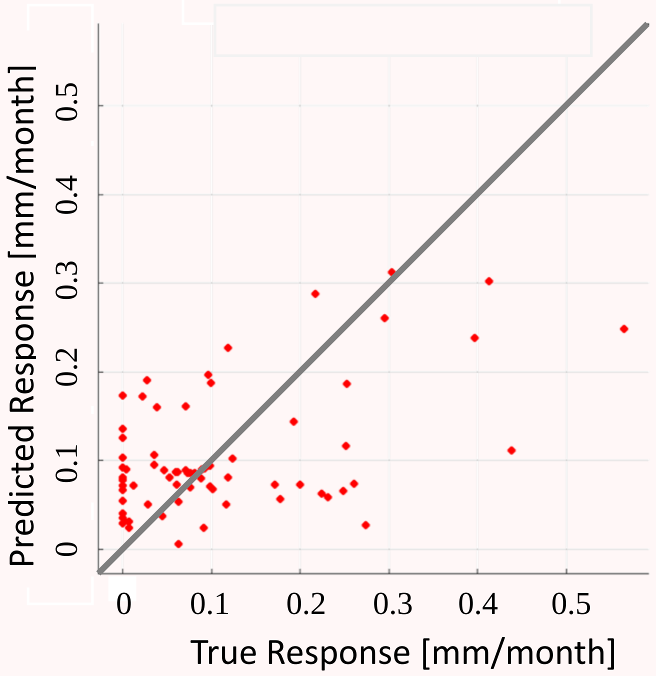

Global shape features (PCA)

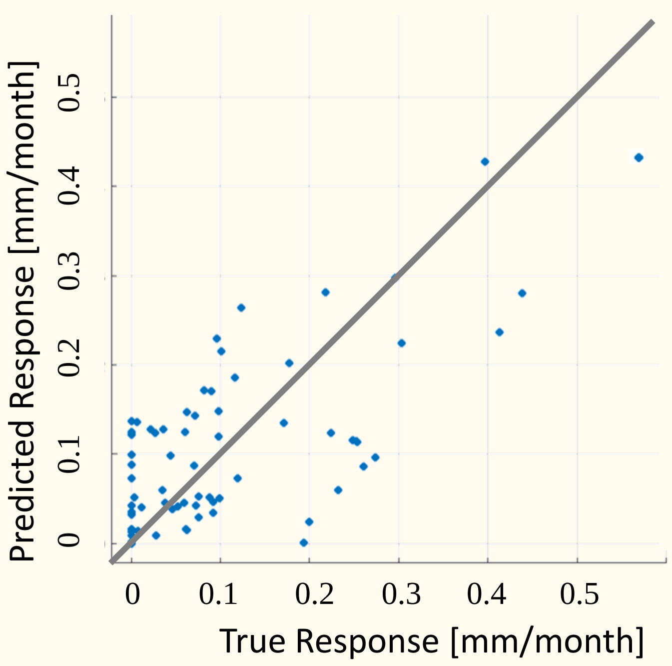

Global shape features (PLS)

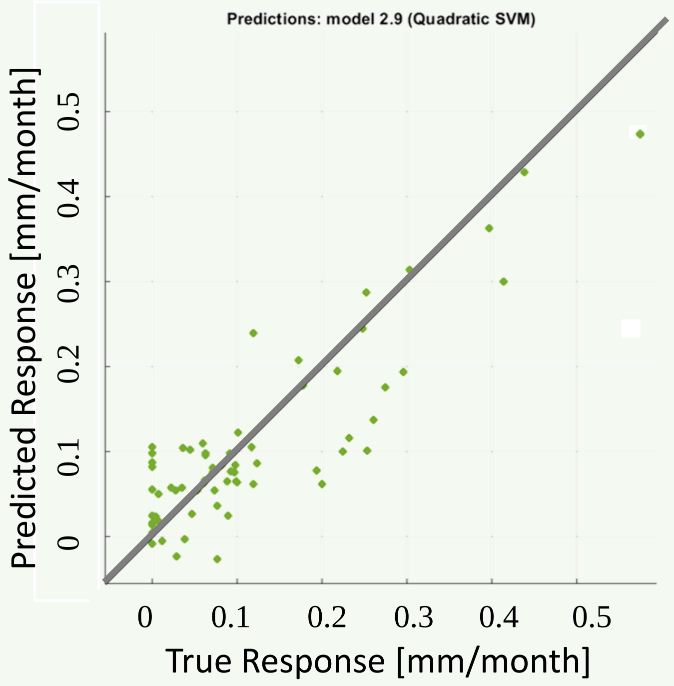

$\boldsymbol{R^2}$ local shape features = 0.28

$\boldsymbol{R^2}$ global shape features (PCA) = 0.42

$\boldsymbol{R^2}$ global shape features (PLS) = 0.63

$\boldsymbol{RMSE}$ local shape features = 0.112 $\frac{mm}{month}$

$\boldsymbol{RMSE}$ global shape features (PCA) = 0.083 $\frac{mm}{month}$

$\boldsymbol{RMSE}$ global shape features (PLS) = 0.066 $\frac{mm}{month}$

Discussion

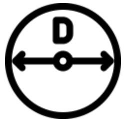

- **Diameter alone fails** to accurately **predict** the aneurysm **growth** according to classifiers used.

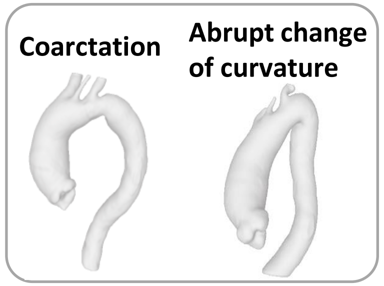

- The use of **diameter** as a criterion for surgery should **not be replaced** by these features, **but** rather **complemented** by them.

- **Shape features alone** are **insufficient** to predict aneurysm growth.

MAIN LIMITATIONS

- The most important limitations are the **small dataset** of patients used, the **unequal distribution** of **classes** for classification.

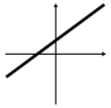

- The assumption of **linear growth** could be valid only for low $\Delta time$.

PART 2

HIGH-FIDELITY AORTA MODELING ACCOUNTING FOR THE HEART MOTION AND THE INTERACTION WITH THE SURROUNDING TISSUES

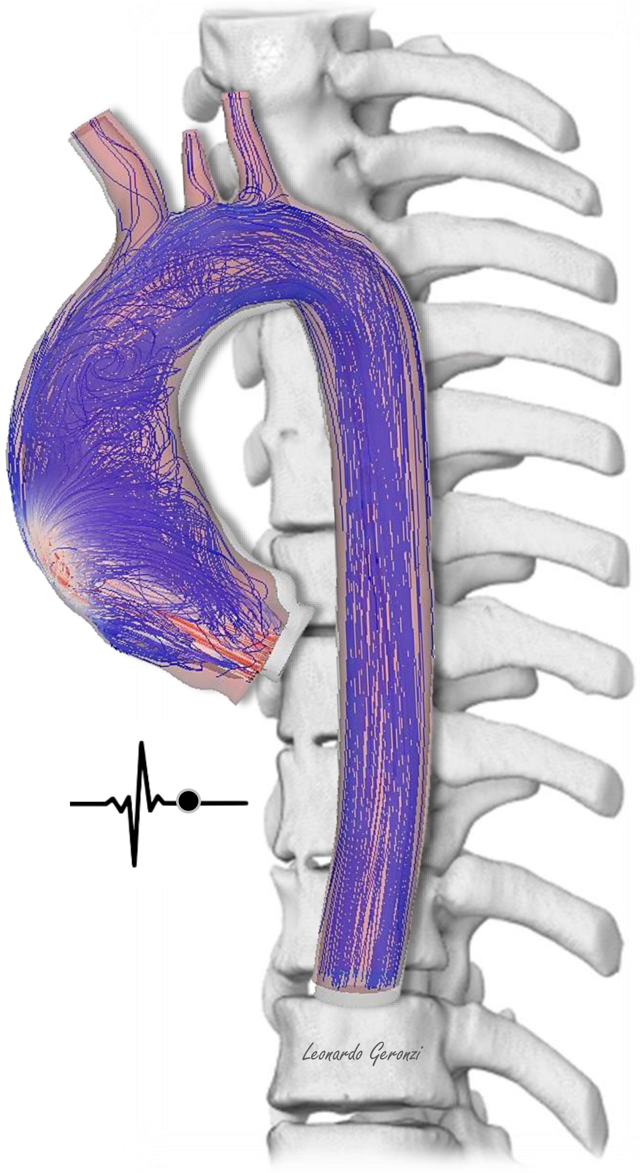

High-Fidelity Modeling

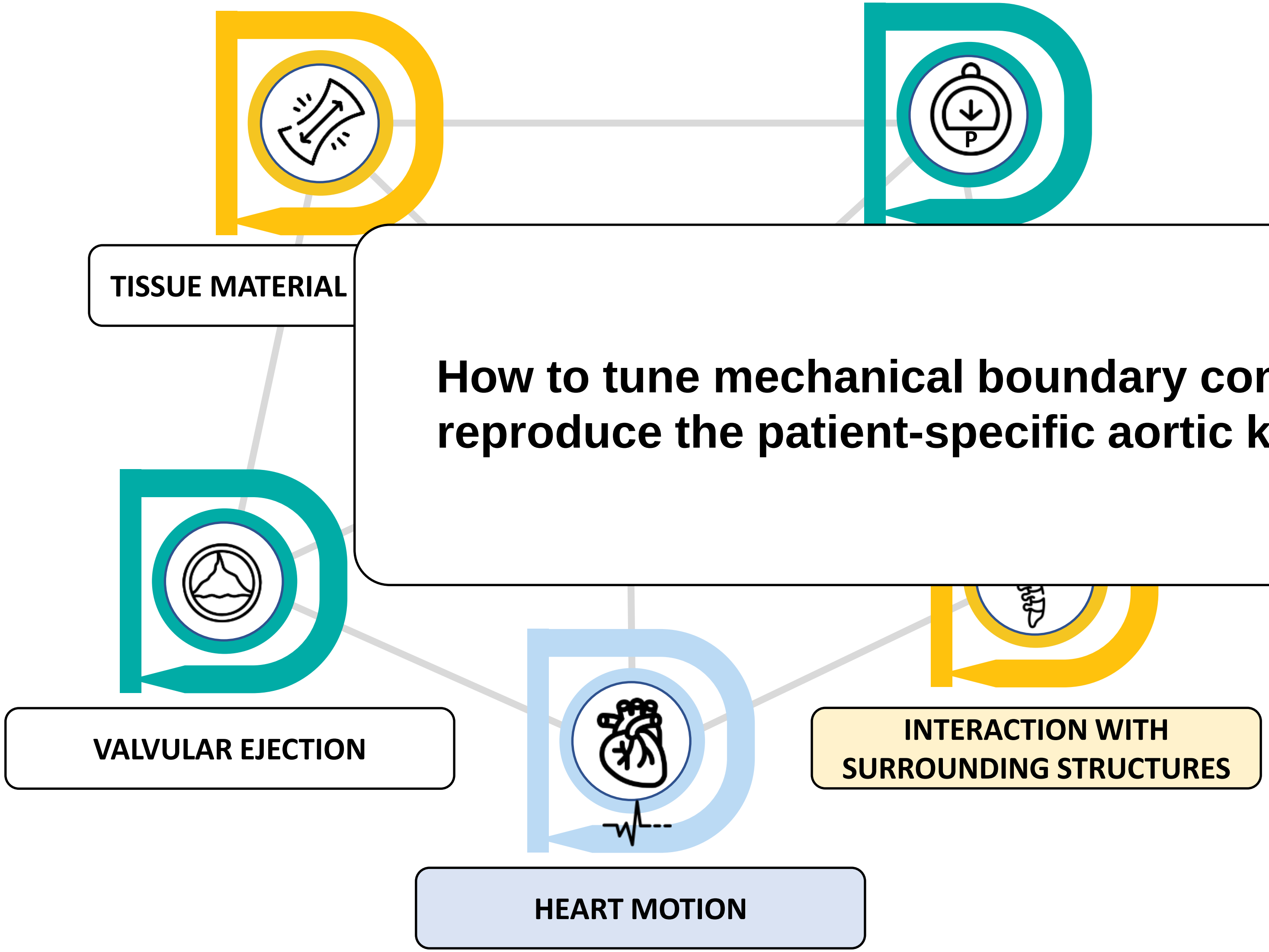

How to tune mechanical boundary conditions to accurately reproduce the patient-specific aortic kinematics?

HEART MOTION

INTERACTION WITH SURROUNDING STRUCTURES

l in
he aorta

mulation
etailed
nesis of
aneurysms and dissections [6].

[6]

Role of Aortic Root Motion in the Pathogenesis of Aortic Dissection
Circulation

Carsten J. Beller, MD, Michel R. Labrosse, PhD, Mano J. Thubrikar, PhD, and Francis Robicsek, MD, PhD

The dataset

ONE DAY BEFORE SURGERY

9 sagittal + 2 oblique sequences

1 **Cine-MRI** — To extract the kinematics of the aorta and detect the valve opening area

2 **MRI Angiography** — To derive the 3D model of the aorta in diastole and the spine

ONE DAY AFTER SURGERY

3 **Experimental Data** — To include patient-specific material properties [7]

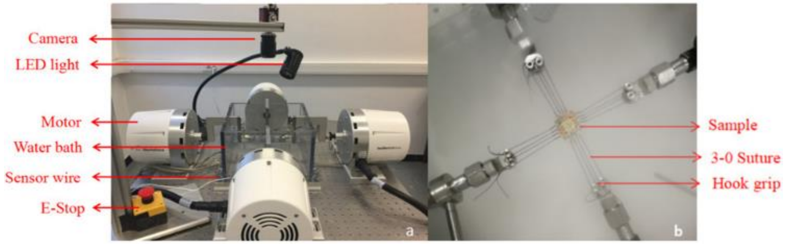

[7] Morgant et al. (2021), *PloS one*, *16*(9), e0256278.

The calibration procedure

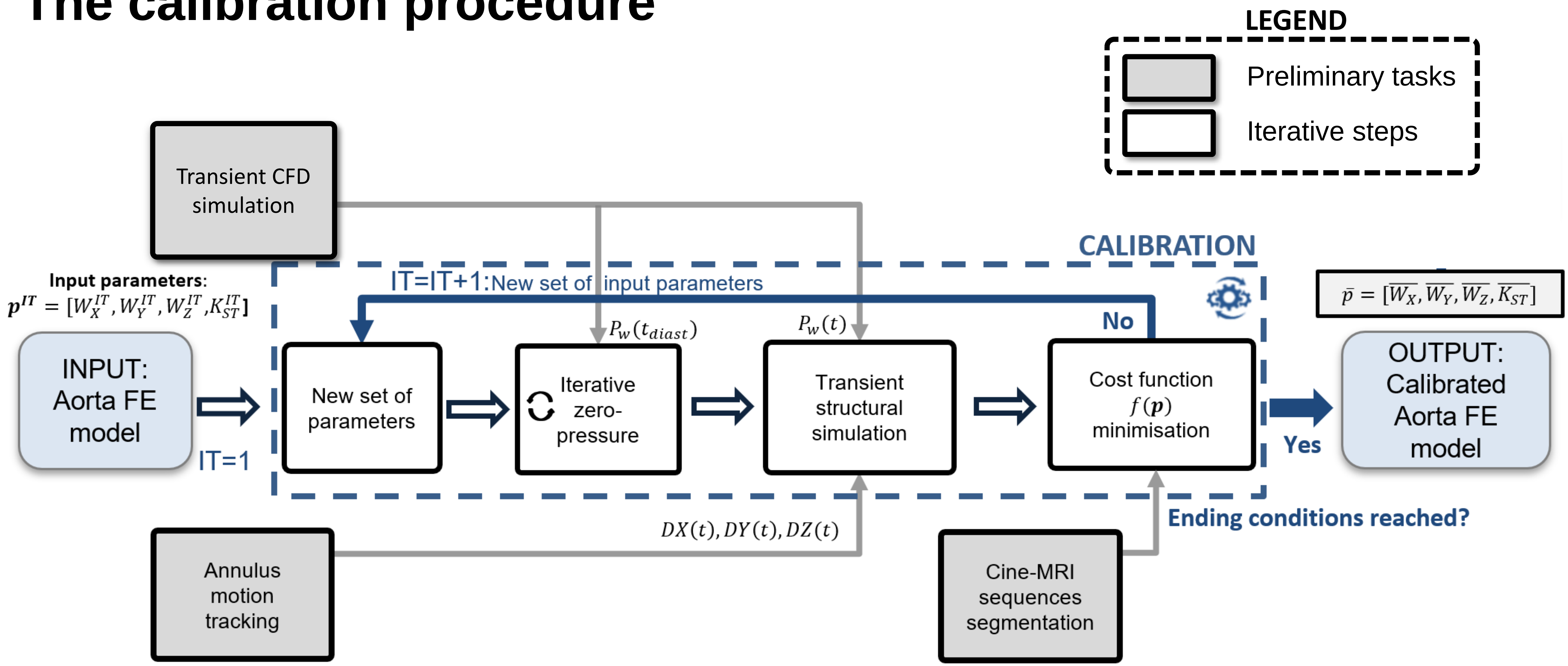

The calibration procedure

Input parameters:
$p^{IT} = [W_X^{IT}, W_Y^{IT}, W_Z^{IT}, K_{ST}^{IT}]$

INPUT:
Aorta FE
model

From **MRI-Angiography**

Local
thresholding

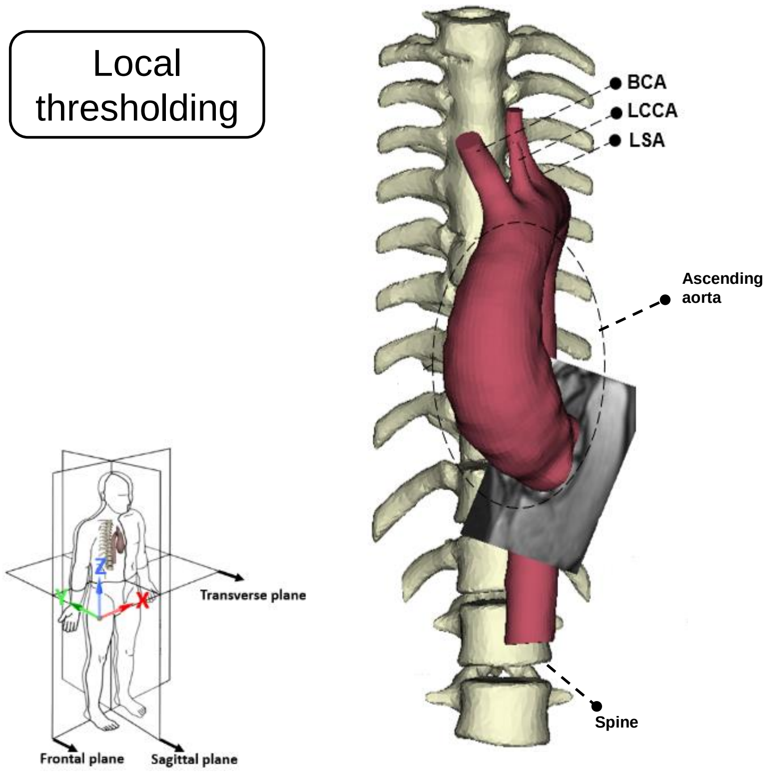

The calibration procedure

Input parameters:
$\boldsymbol{p}^{IT} = [W_X^{IT}, W_Y^{IT}, W_Z^{IT}, K_{ST}^{IT}]$

INPUT: Aorta FE model

Shell elements

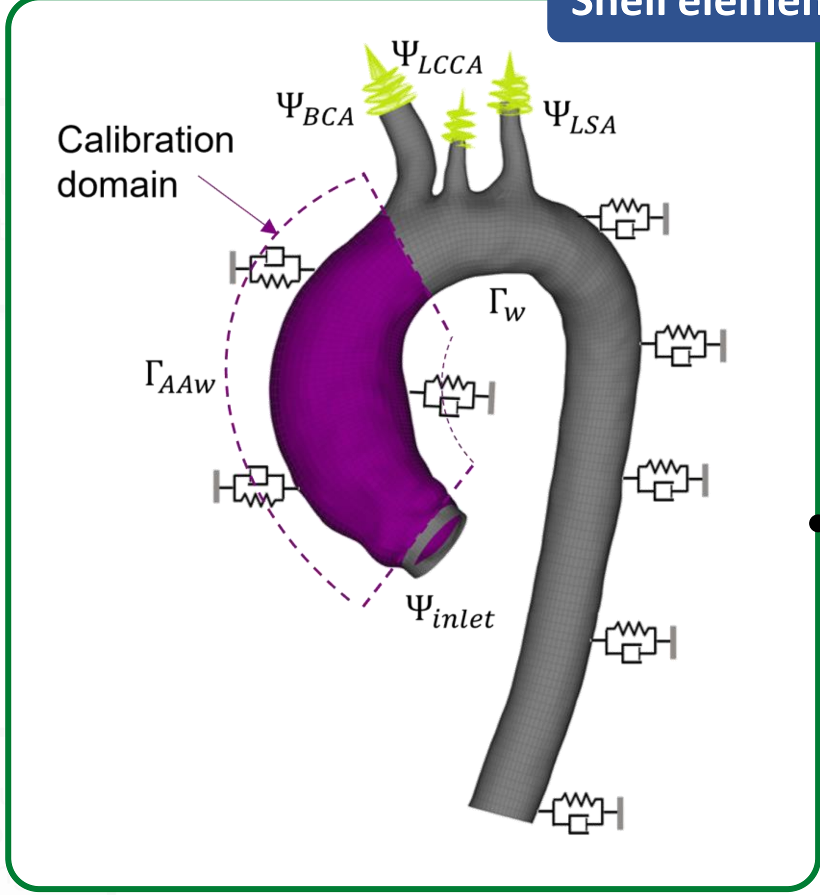

Hyperelastic material model:
3-parameters Mooney-Rivlin

Robin Boundary Conditions [5]

$$\boldsymbol{\sigma}_{\mathbf{ext}} = -\mathbf{Kx} - \eta\dot{\mathbf{x}}$$

$$K_{X_i} = K_{ST} + (W_{d_i} W_X) K_{SPINE}$$
$$K_{Y_i} = K_{ST} + (W_{d_i} W_Y) K_{SPINE}$$
$$K_{Z_i} = K_{ST} + (W_{d_i} W_Z) K_{SPINE}$$

$W_{d_i} = 1 - \alpha \dfrac{d_i}{d_{MAX}}$ $\quad d_{MAX} = 142$ mm $\quad \alpha = 0.95$

$\eta = 10^5\ (Pa \cdot s)/m$ $\quad K_{SPINE} = 10^6\ Pa/m$

Input parameters: $\boldsymbol{p} = [W_X, W_Y, W_Z, K_{ST}]$ **to be tuned**

The initial value of the parameters was $\mathbf{p}^1 = [1, 1, 1, 1 \times 10^5$ Pa/m] [8,9]

[8] Moireau et al. (2012), *Biomechanics and modeling in mechanobiology*, *11*(1), 1-18.

[9] Gindre et al. (2016), *IEEE Transactions on Biomedical Engineering* 64.5 1057-1066.

The calibration procedure

Transient CFD simulation

Input parameters:
$\boldsymbol{p}^{IT} = [W_X^{IT}, W_Y^{IT}, W_Z^{IT}, K_{ST}^{IT}]$

INPUT:
Aorta FE model

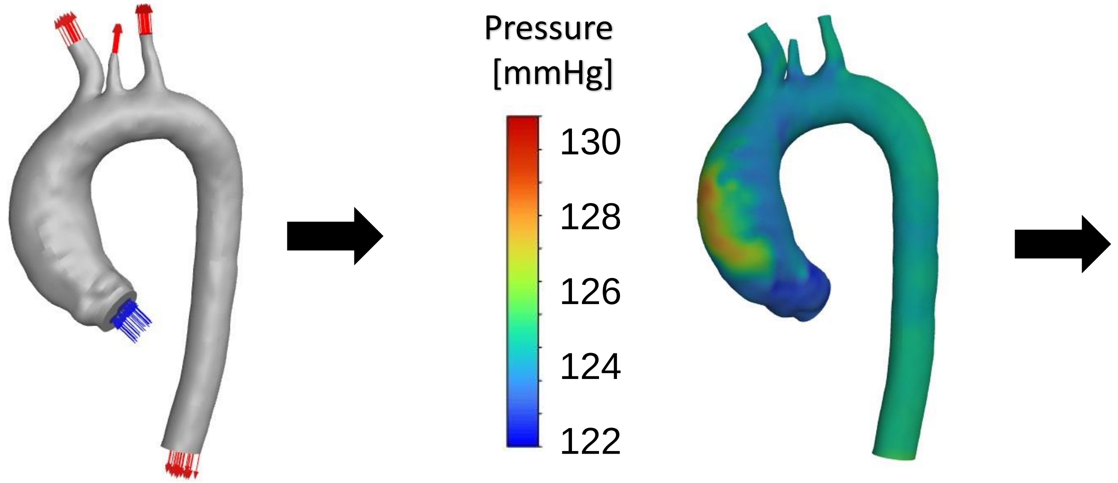

$\boldsymbol{P_w(t)}$ mapped on the structural wall

The calibration procedure

Transient CFD simulation

Input parameters:

$$\boldsymbol{p}^{IT} = [W_X^{IT}, W_Y^{IT}, W_Z^{IT}, K_{ST}^{IT}]$$

INPUT: Aorta FE model

Annulus motion tracking

Repeating it for all the slices

Extracting the average

RIGID BODY MOTION (mid-point)

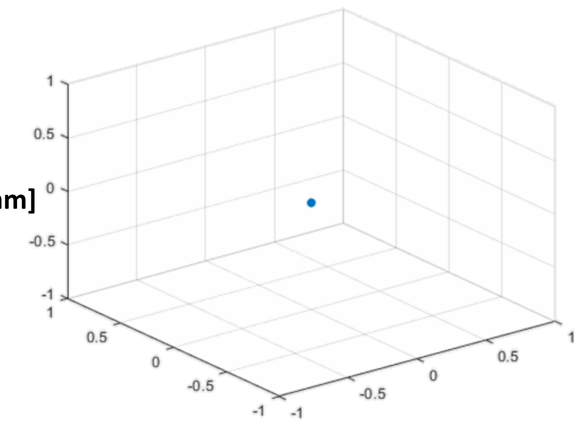

The calibration procedure

Transient CFD simulation

Input parameters:
$$p^{IT} = [W_X^{IT}, W_Y^{IT}, W_Z^{IT}, K_{ST}^{IT}]$$

INPUT: Aorta FE model

Annulus motion tracking

From **cine-MRI**

9 sagittal + 2 oblique sequences

Region Growing

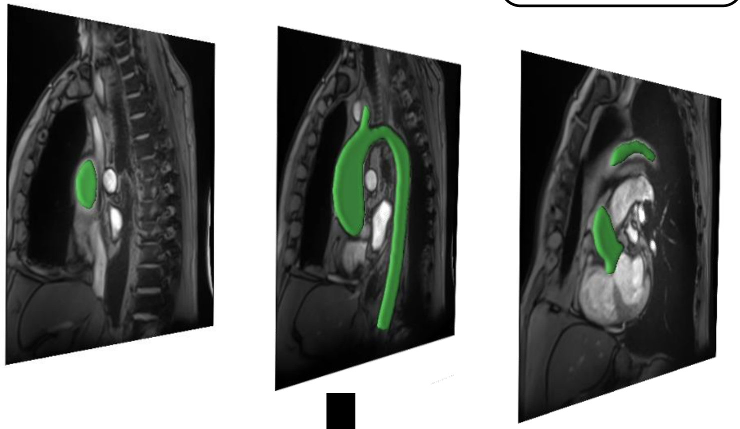

The wall positions during the cardiac cycle were extracted

Cine-MRI sequences segmentation

The calibration procedure

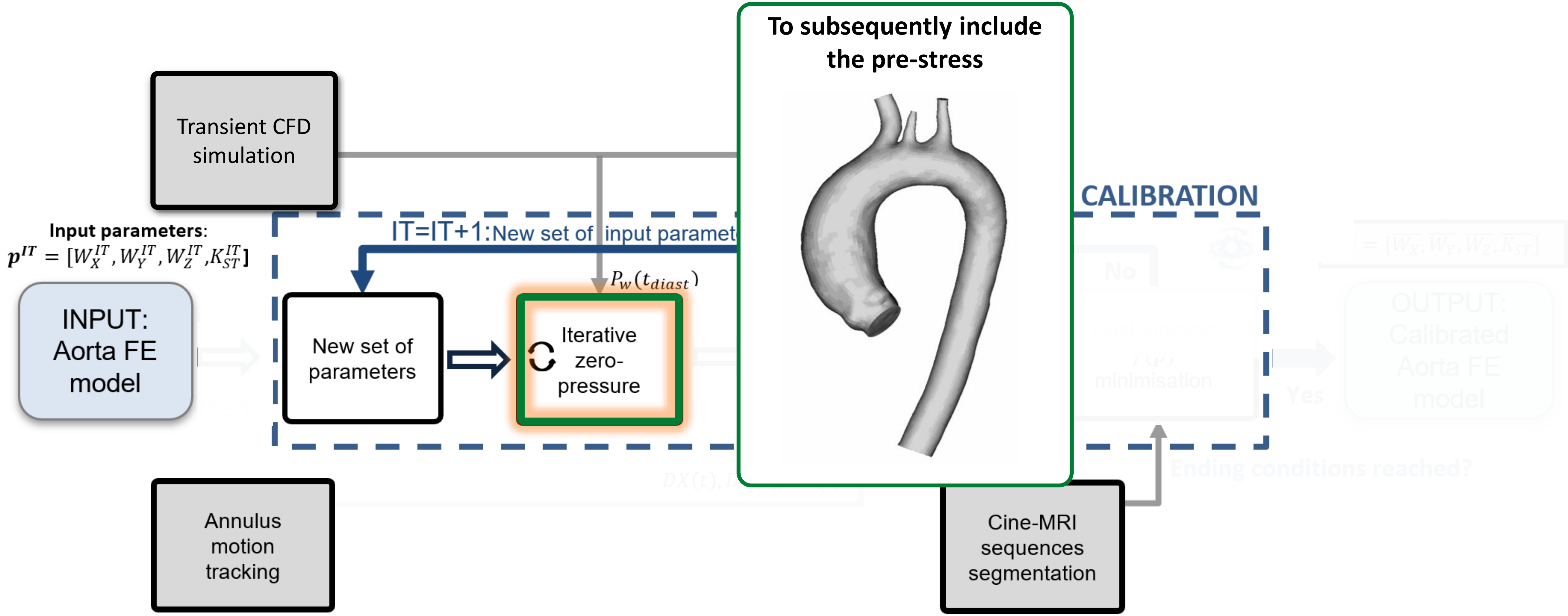

The calibration procedure

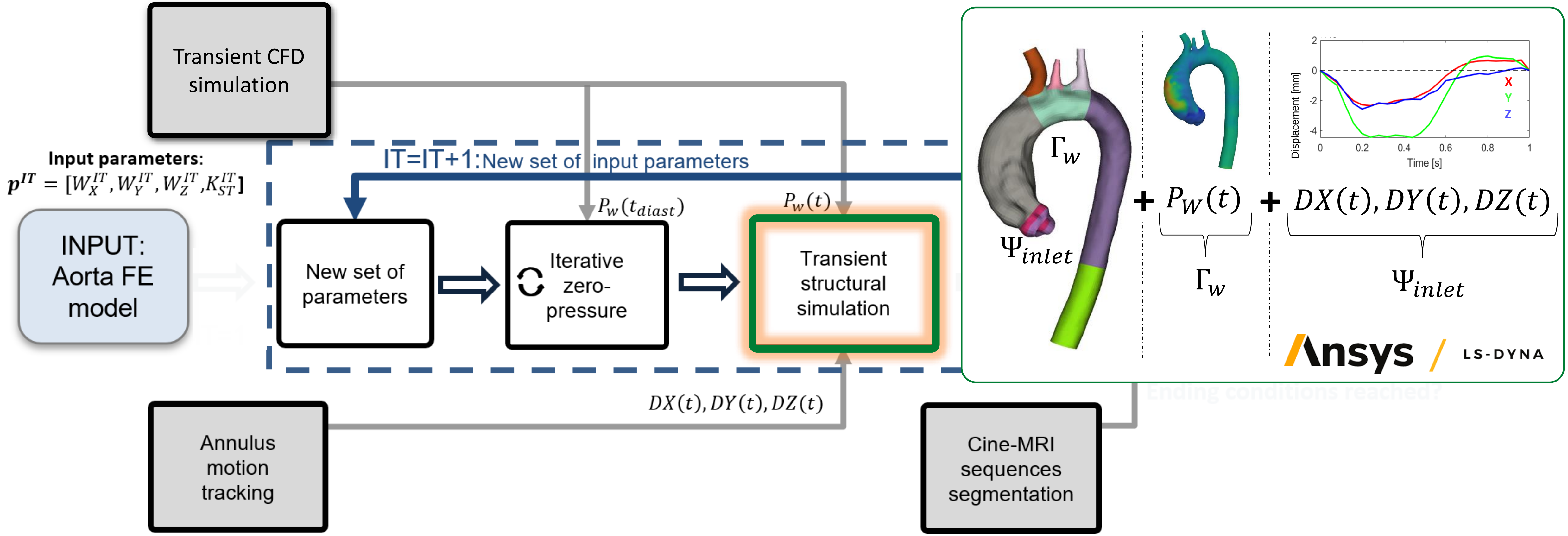

The calibration procedure

- Calibration criterion: matching between the splines obtained by intersecting the cine-MRI planes and the deformed FE model and the splines obtained from the boundaries of the cine-MRI segmentations.

$$f(\mathbf{p}) = \sqrt{\sum_{\varphi}\sum_{l=1}^{m}\sum_{k=1}^{n_l}\left|d_{l,k}^{\varphi}(\mathbf{p})\right|^2}$$

$$d_{l,k}^{\varphi}(\mathbf{p}) = d(\mathbf{x}_{l,k}^{\varphi}, \mathbf{S}_l^{\varphi}(\mathbf{p})) = \min_{\mathbf{x}_{sim} \in \mathbf{S}_l^{\varphi}(\mathbf{p})} \left\|\mathbf{x}_{l,k}^{\varphi} - \mathbf{x}_{sim}\right\|$$

- φ = number of cine-MRI frames
- *m* = 11 is the number splines from the images
- n_l = the number of points for the l-spline
- $d_{l,k}^{\varphi}$ = nearest neighbour distance between the simulation-derived splines and the splines from cine-MRI

- **Levenberg-Marquardt (LM) least-squares optimization.**

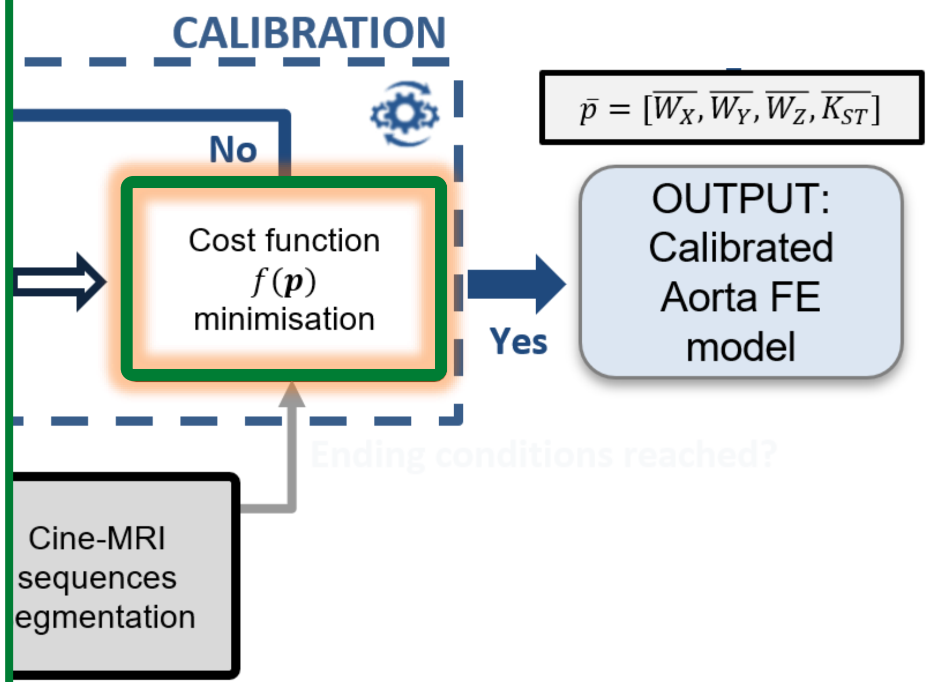

Calibration Results

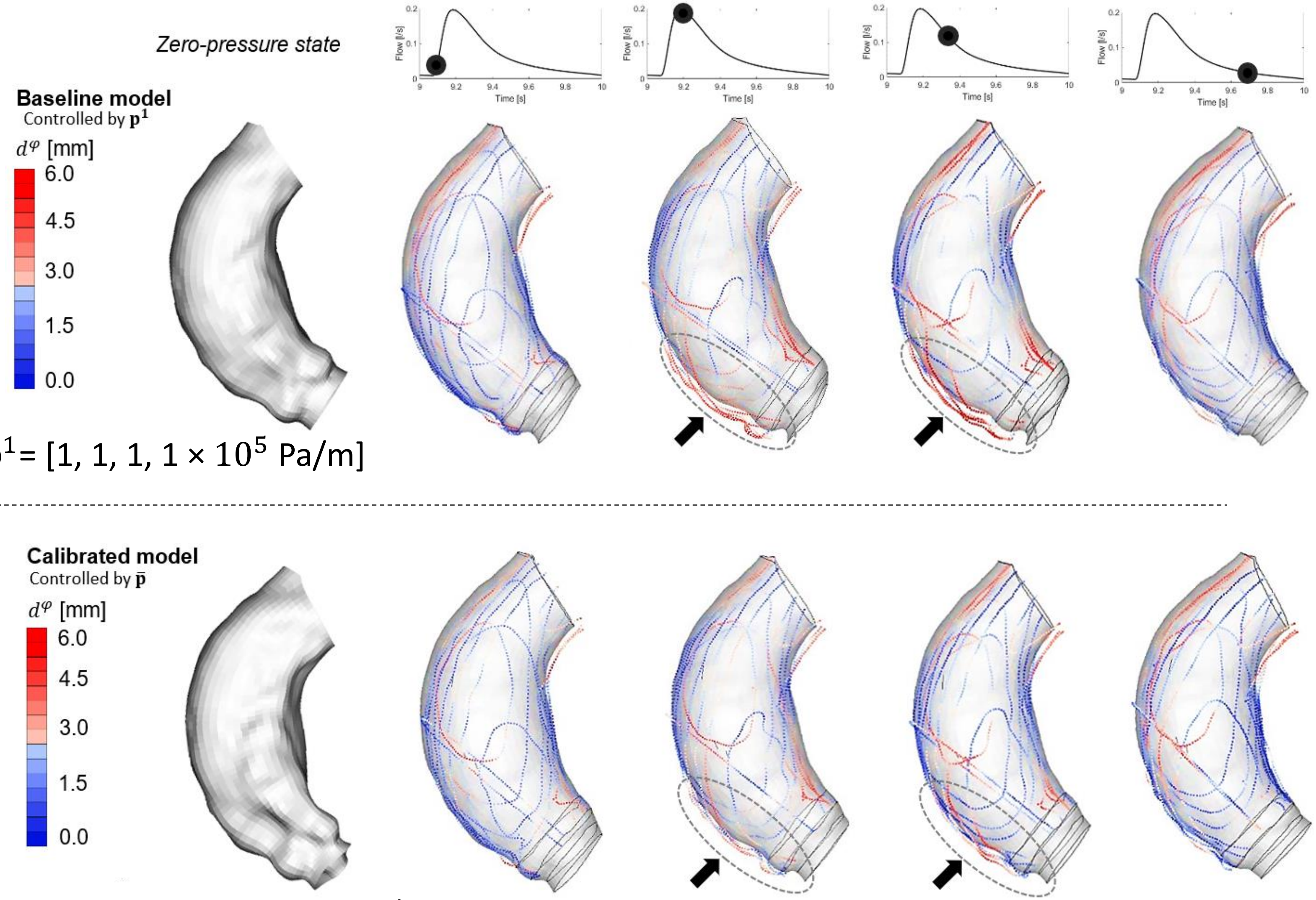

$\mathbf{p}^1$= [1, 1, 1, 1 × 10^5 Pa/m]

$\bar{\mathbf{p}}$= [0.6, 0.02, 0.04, 1.5 × 10^4 Pa/m]

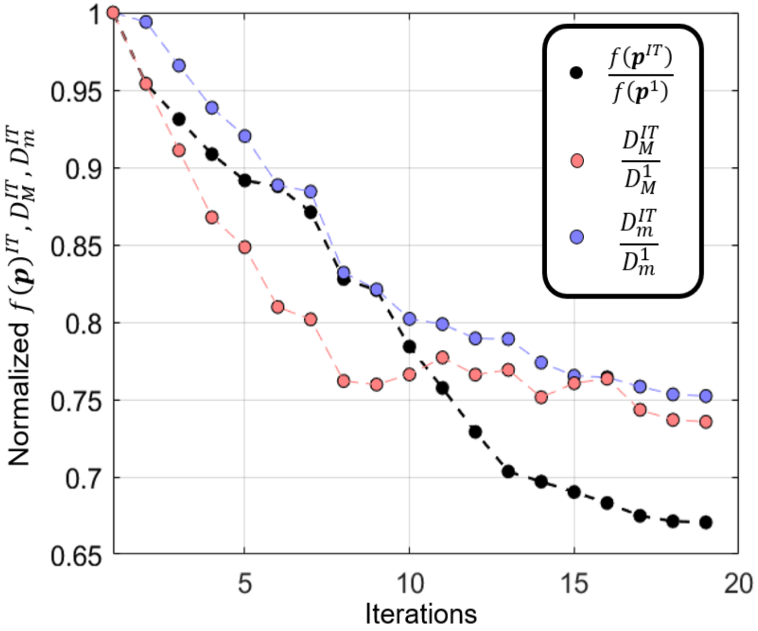

$f(\mathbf{p})$ was reduced by 34% after 19 iterations

Maximum distance D_M: 8.64 mm → 6.37 mm

Mean distance D_m: 2.24 mm → 1.83 mm

Computational time: 32 hours: 32-cores, parallel

Calibration Results

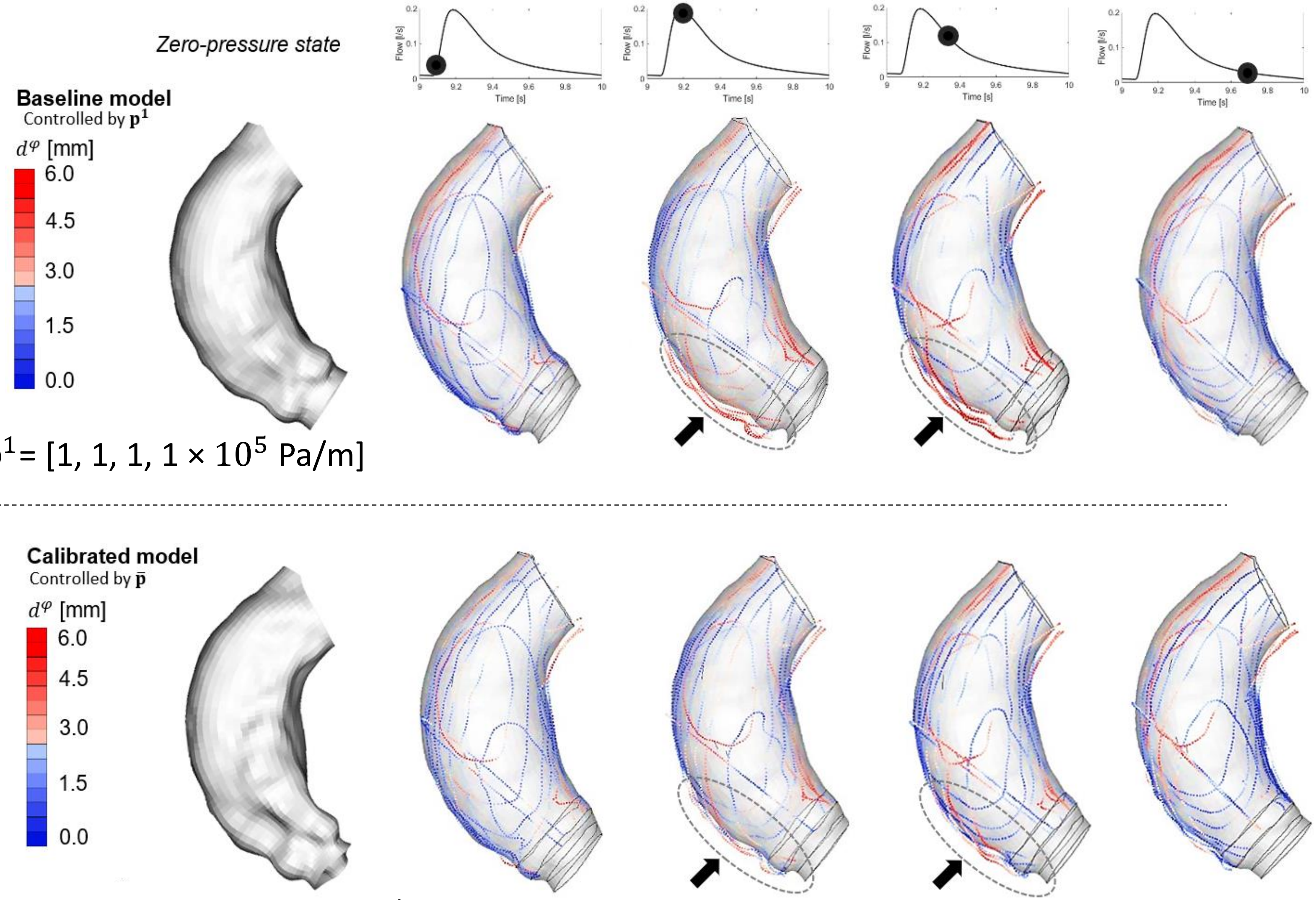

$\mathbf{p}^1$= [1, 1, 1, 1 × 10^5 Pa/m]

$\bar{\mathbf{p}}$= [0.6, 0.02, 0.04, 1.5 × 10^4 Pa/m]

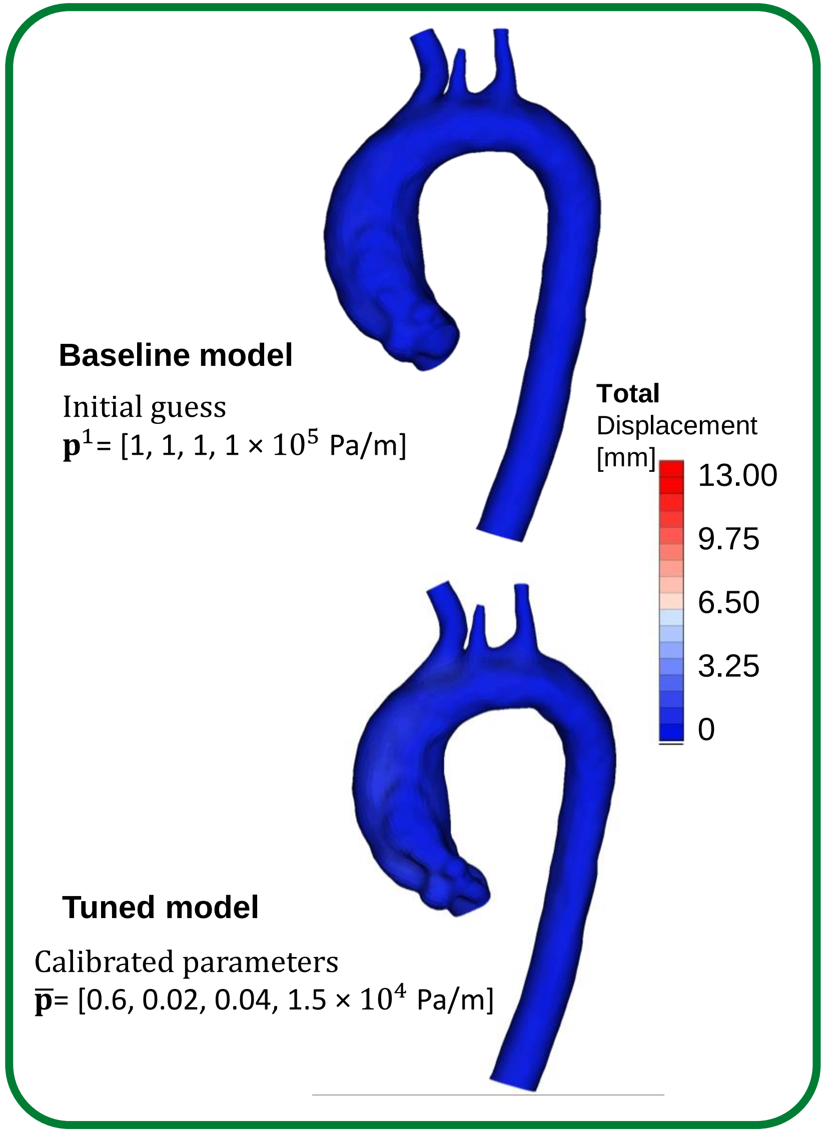

Discussion

- ❑ The model with the tuned BCs is able to reproduce the real wall displacement more faithfully than without calibrated parameters.

Higher fidelity in reproducing the real kinematics vessel behaviour → Better assessment of quantities such as strain and stress → More accurate prediction of events such as aneurysm growth and dissection [10]

MAIN LIMITATIONS

- ❑ It is not easy to extend the workflow to other patients.

- ❑ It is really complex to reduce the error (i.e., the cost function) to 0: one of the reasons is that the wall BCs were controlled by only 4 parameters related to the stiffnesses.

$$\boldsymbol{\sigma}_{\mathbf{ext}} = -\boxed{\mathbf{K}}\mathbf{x} - \eta\dot{\mathbf{x}}$$

[10] Beller et al. *Journal of medical engineering & technology* 32.2 (2008): 167-170.

PART 3

HEMODYNAMIC REAL-TIME PREDICTION BASED ON SURROGATE MODELING TECHNIQUES

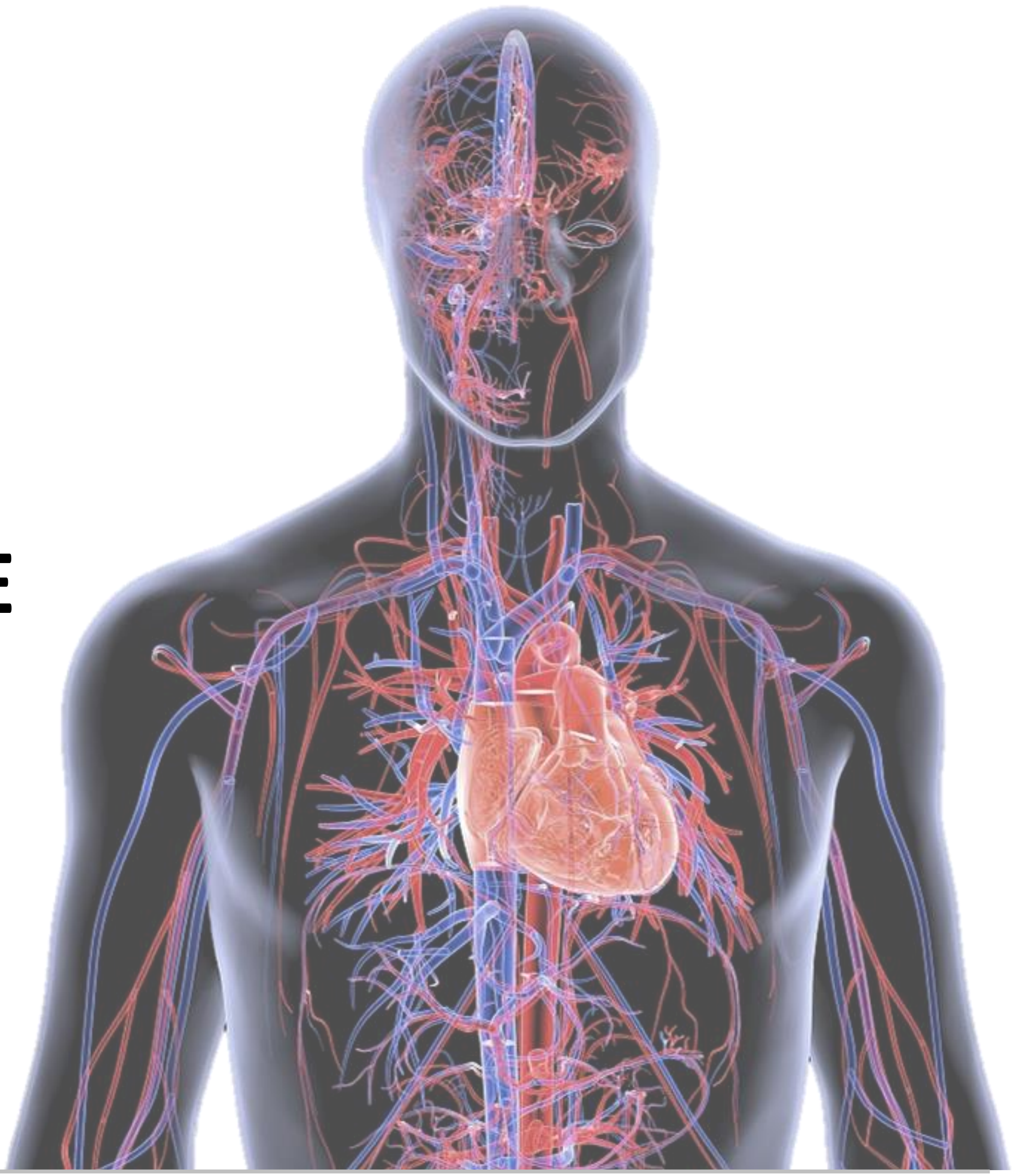

Hemodynamic prediction based on surrogate modeling

OFFLINE PHASE

n_p — Extraction of the geometries → $n_p - 1$ — Alignement to the template → $n_p - 1$ — Creation of iso-topological grids → n_{vp} — Generation of the atlases → n_{vp} — Creation of the CFD snapshots

Iterative Closest Point

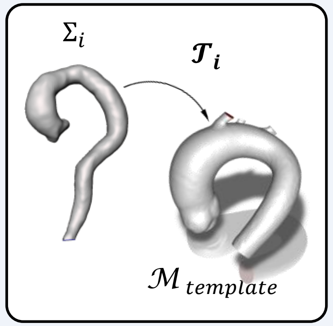

RBF mesh morphing

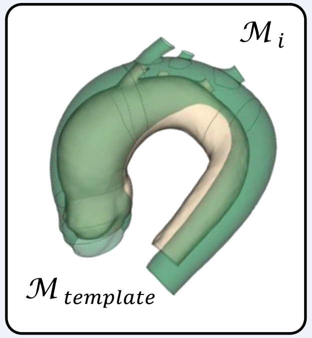

Statistical Shape Modeling

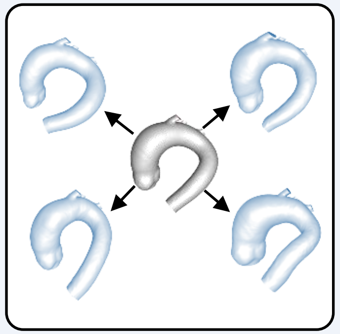

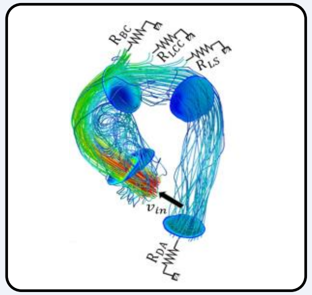

1 left-out patient — Geometry exclusion

Building of the ROM

Response Surface method

SURROGATE MODEL

ONLINE PHASE

1 left-out patient — Alignment to the template → *RBF mesh morphing* → 1 left-out patient — Creation of iso-topological grid → *Least squares fitting* → Shape coefficients determination → Low-order solution

Automatic CFD simulations → High-order solution → **Validation** for the left-out patient

FULL ORDER SIMULATION

The offline phase [1/2]

MRI 4D Flow

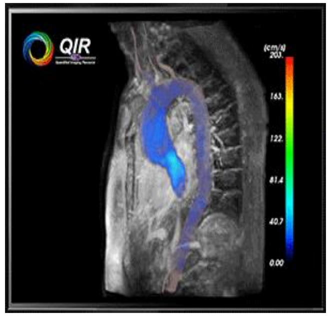

Automatic (3D U-net) segmentation methods developed by Marin-Castrillon et al. [11]

⇨ **3D model**

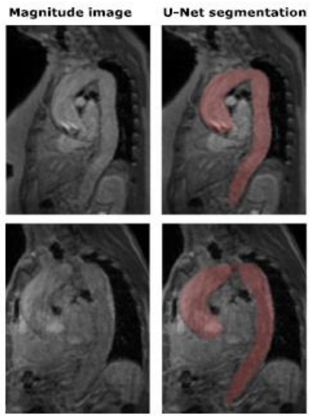

[11] Marin-Castrillon et al. *Magnetic Resonance Materials in Physics, Biology and Medicine* (2023): 1-14.

The offline phase [1/2]

MRI 4D Flow

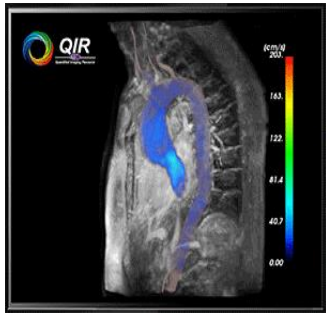

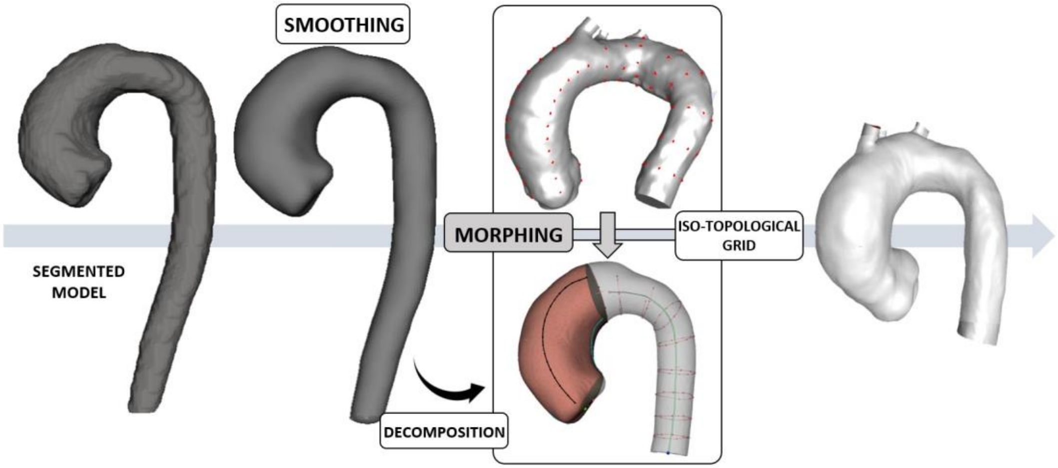

Automatic (3D U-net) segmentation methods developed by Marin-Castrillon et al. [11] ⇨ **3D model** ⇨ **RBF Mesh Morphing** ⇨ **Iso-topological grid**

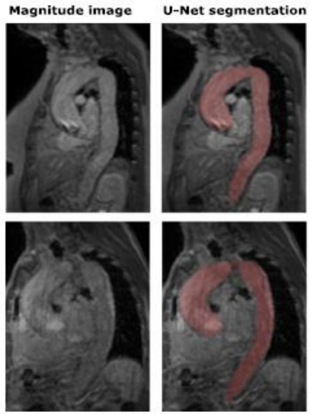

$$s(\mathbf{x}) = \sum_{i=1}^{N} \gamma_i \varphi\left(\left\|\mathbf{x} - \mathbf{x}_{\mathbf{s_i}}\right\|\right) + h(\mathbf{x})$$

In the 3D space:

$$\mathbf{x}_{\mathbf{node_{new}}} = \mathbf{x}_{\mathbf{node}} + \begin{bmatrix} s_x(\mathbf{x}_{\mathbf{node}}) \\ s_y(\mathbf{x}_{\mathbf{node}}) \\ s_z(\mathbf{x}_{\mathbf{node}}) \end{bmatrix}$$

[11] Marin-Castrillon et al. *Magnetic Resonance Materials in Physics, Biology and Medicine* (2023): 1-14.

The offline phase [1/2]

MRI 4D Flow

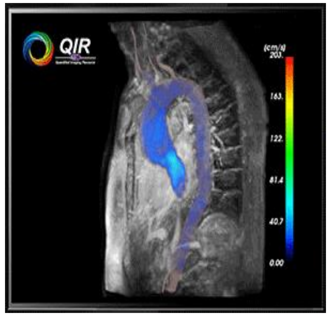

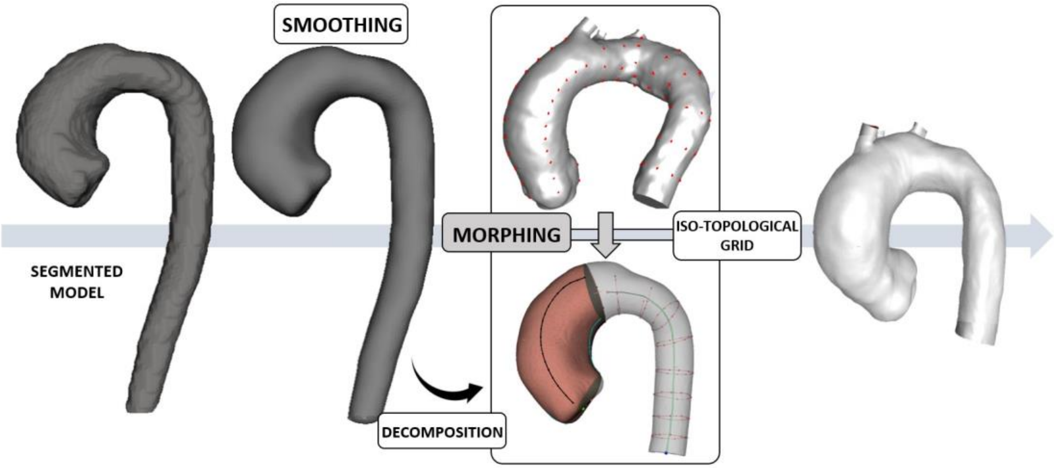

Based on principal component analysis (**PCA**)

Each shape $\widetilde{M_S}^i$ can be built combining n_{SM} eigenvalues λ_j and n_{SM} eigenvectors $\boldsymbol{W_j}$

$$\widetilde{M_S}^i = M_{S_{mean}} + \sum_{j=1}^{n_{SM}} c_j^i \sqrt{\lambda_j}\mathbf{W}_j$$

Automatic (3D U-net) segmentation methods developed by Marin-Castrillon et al. [11] → **3D model** → **RBF Mesh Morphing** → **Iso-topological grid** → **Statistical Shape Modeling** → **Parametric 3D model**

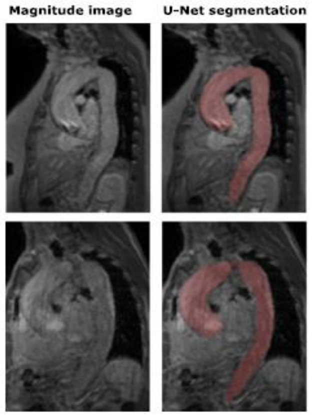

$$s(\mathbf{x}) = \sum_{i=1}^{N} \gamma_i \varphi\left(\left\|\mathbf{x} - \mathbf{x}_{s_i}\right\|\right) + h(\mathbf{x})$$

In the 3D space:

$$\mathbf{x}_{\mathbf{node}_{\mathbf{new}}} = \mathbf{x}_{\mathbf{node}} + \begin{bmatrix} s_x(\mathbf{x}_{\mathbf{node}}) \\ s_y(\mathbf{x}_{\mathbf{node}}) \\ s_z(\mathbf{x}_{\mathbf{node}}) \end{bmatrix}$$

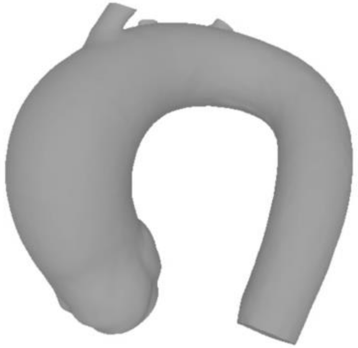

[11] Marin-Castrillon et al. *Magnetic Resonance Materials in Physics, Biology and Medicine* (2023): 1-14.

The offline phase [2/2]

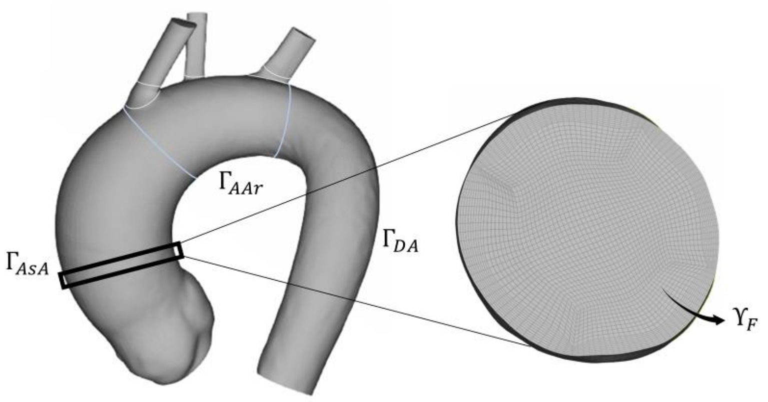

CFD Simulation using the synthetic data created through SSM → **Set of learning snapshots (Wall pressure)**

Navier-Stokes equations:

$$\mathbf{u} \cdot \nabla \mathbf{u} = -\frac{1}{\rho} \nabla p + \nu \nabla^2 \mathbf{u}, \text{ in } \Upsilon_F$$

$$\nabla \cdot \mathbf{u} = 0, \text{ in } \Upsilon_F$$

SIMPLE pressure-velocity coupling

Parameteric velocity **inlet** – pressure **outlet** BCs

The offline phase [2/2]

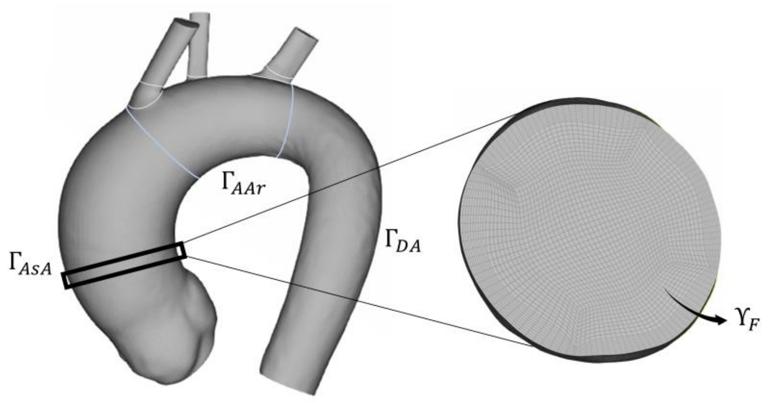

1) DECOMPOSITION

Proper orthogonal decomposition (**POD**) techniques:

$$\mathbf{\Omega} = \boldsymbol{U\Sigma V^T}$$

$$\min_{\mathbf{\Phi}} \left\| \mathbf{\Omega} - \mathbf{\Phi}\mathbf{\Phi}^{\mathbf{T}} \right\|^2$$

CFD Simulation using the synthetic data created through SSM → **Set of learning snapshots (Wall pressure)** → **Model order reduction techniques** → **Surrogate Model**

Navier-Stokes equations:

$$\mathbf{u} \cdot \nabla \mathbf{u} = -\frac{1}{\rho} \nabla \mathrm{p} + \nu \nabla^2 \mathbf{u}, \text{in } \Upsilon_{\mathrm{F}}$$

$$\nabla \cdot \mathbf{u} = 0, \text{in } \Upsilon_{\mathrm{F}}$$

SIMPLE pressure-velocity coupling

Parameteric velocity **inlet** – pressure **outlet** BCs

2) INTERPOLATION

Genetic Aggregation Response Surface (**GARS**) technique for the ROM interpolation

19 Geometrical parameters

5 Physical parameters

The offline phase [2/2]

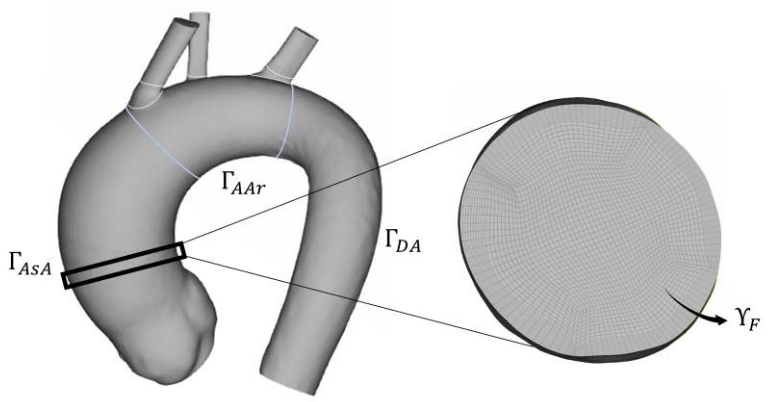

1) DECOMPOSITION

Proper orthogonal decomposition (**POD**) techniques:

$$\boldsymbol{\Omega} = \boldsymbol{U\Sigma V^T}$$

$$\min_{\boldsymbol{\Phi}} \left\| \boldsymbol{\Omega} - \boldsymbol{\Phi\Phi}^{\mathbf{T}} \right\|^2$$

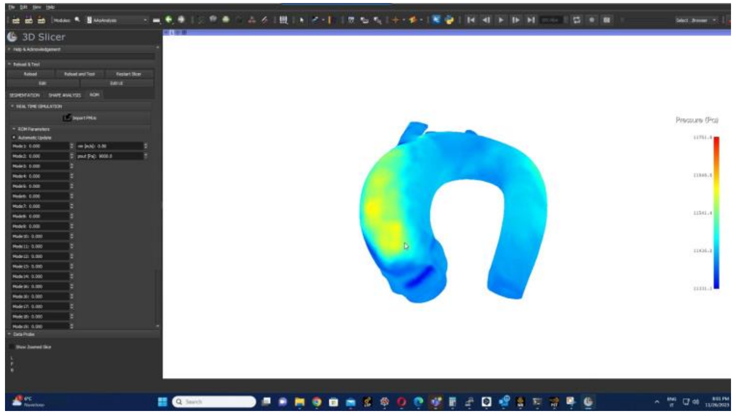

CFD Simulation using the synthetic data created through SSM → **Set of learning snapshots (Wall pressure)** → **Model order reduction techniques** → **Surrogate Model** → **Surrogate model deployment**

Navier-Stokes equations:

$$\mathbf{u} \cdot \nabla \mathbf{u} = -\frac{1}{\rho} \nabla p + \nu \nabla^2 \mathbf{u}, \text{in } \Upsilon_F$$

$$\nabla \cdot \mathbf{u} = 0, \text{in } \Upsilon_F$$

SIMPLE pressure-velocity coupling

Parameteric velocity **inlet** – pressure **outlet** BCs

2) INTERPOLATION

Genetic Aggregation Response Surface (**GARS**) technique for the ROM interpolation

- **19** Geometrical parameters
- **5** Physical parameters

FMU DEPLOYMENT
Model Exchange 2.0

The online phase

Excluded patient

Automatic (3D U-net) segmentation

⇩

3D model

The online phase

Excluded patient

Automatic (3D U-net) segmentation

⇓

3D model

⇓

RBF Mesh Morphing ⇒ Iso-topological grid

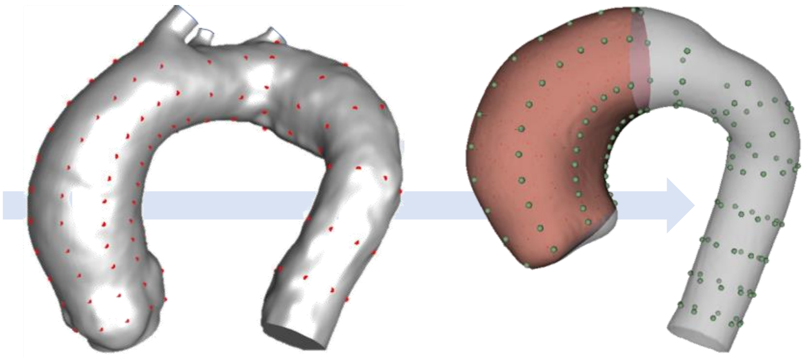

The online phase

Excluded patient

Automatic (3D U-net) segmentation

3D model

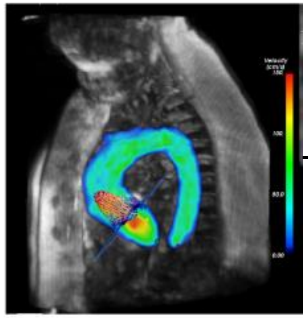

Inlet BC velocity value from the images

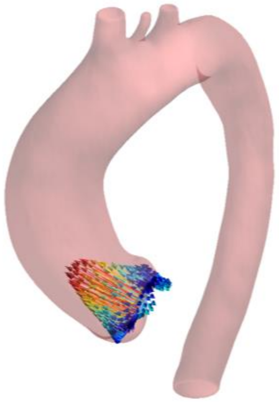

$$\omega^{FOM}(\alpha, \beta) \approx \omega^{ROM}(\alpha, \beta) = \sum_{i=1}^{N_{POD}} w_i \sqrt{\sigma_i(\alpha, \beta)} \phi_i(\alpha, \beta)$$

RBF Mesh Morphing → **Iso-topological grid** → **Shape representation using lest squares fitting** + **ROM interpolation** → **Reduced order results**

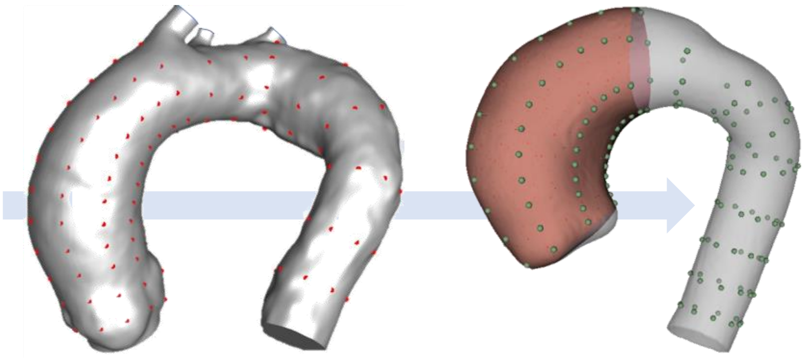

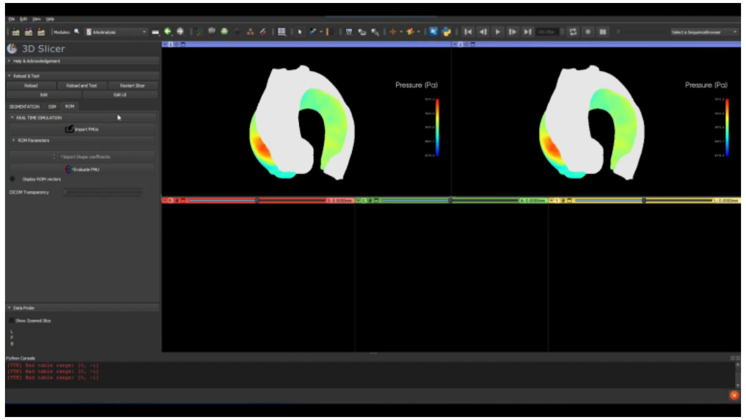

The online phase

Excluded patient

Automatic (3D U-net) segmentation

⇩

3D model

⇩

RBF Mesh Morphing ⇨ Iso-topological grid ⇨ Shape representation using lest squares fitting + ROM interpolation ⇨ Reduced order results ⇨ Comparison full order vs reduced order simulation

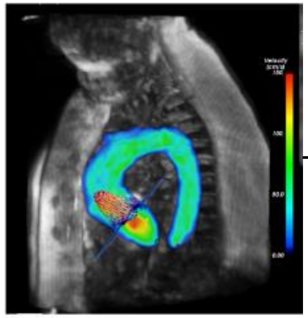

Inlet BC velocity value from the images →

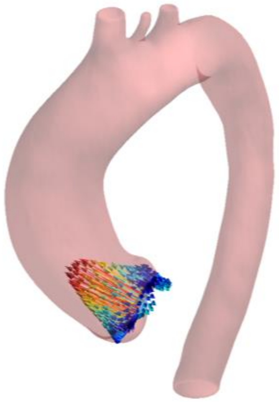

$$\omega^{FOM}(\alpha,\beta) \approx \omega^{ROM}(\alpha,\beta) = \sum_{i=1}^{N_{POD}} w_i \sqrt{\sigma_i(\alpha,\beta)}\,\phi_i(\alpha,\beta)$$

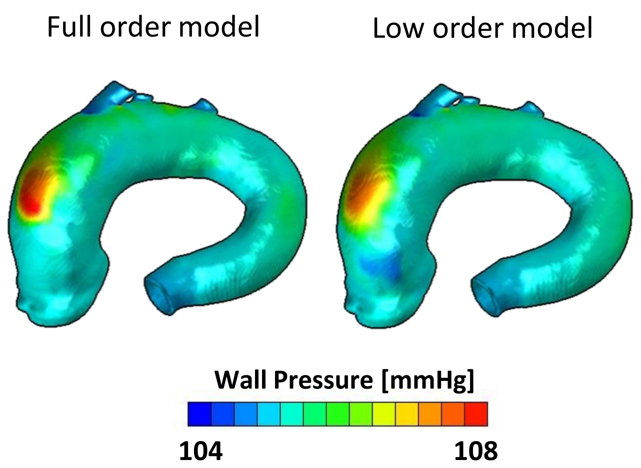

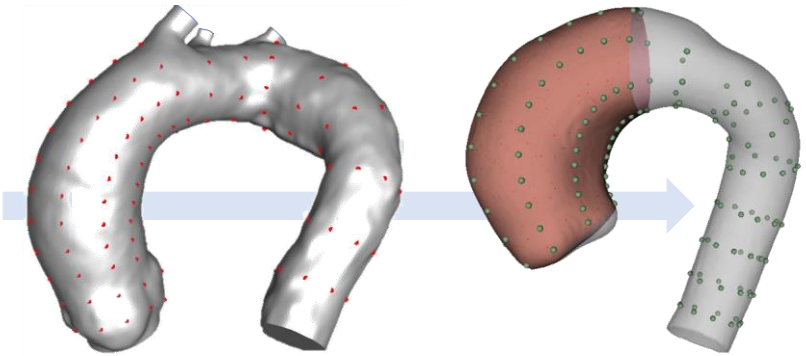

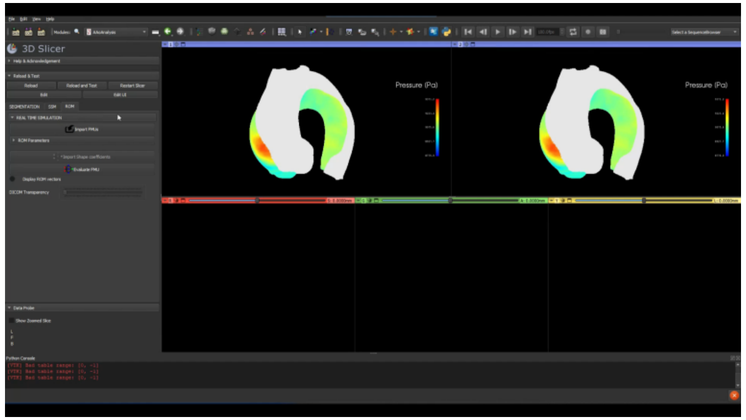

$$e_{ROM}^{rel,i-out} = \frac{\left\|\omega_{i-out}^{FOM} - \omega_{i-out}^{ROM}\right\|}{\left\|\omega_{i-out}^{ROM}\right\|}$$

$$e_{ROM}^{abs,i-out} = \max\left(\left\|\omega_{i-out}^{FOM} - \omega_{i-out}^{ROM}\right\|\right)$$

Leave-one-patient-out validation results

Shape reconstruction by least squares fitting

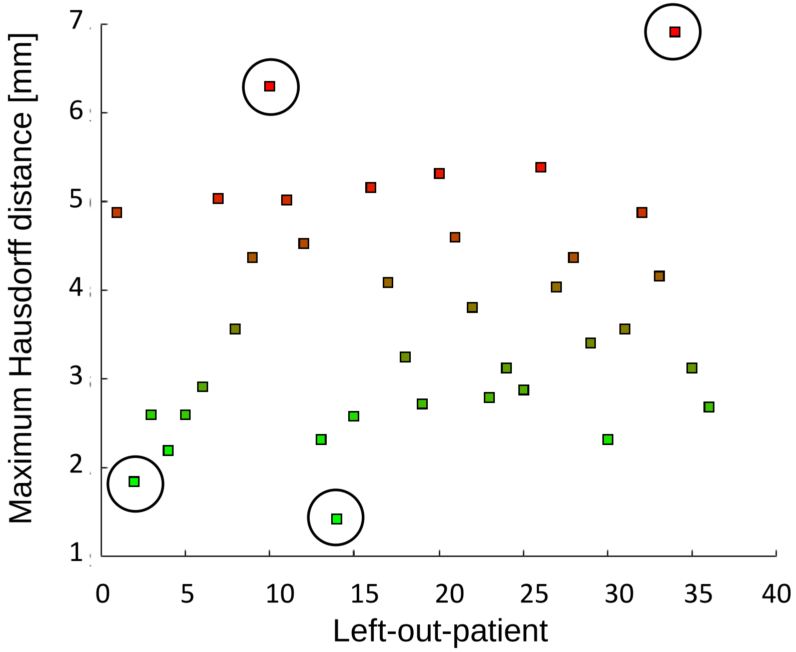

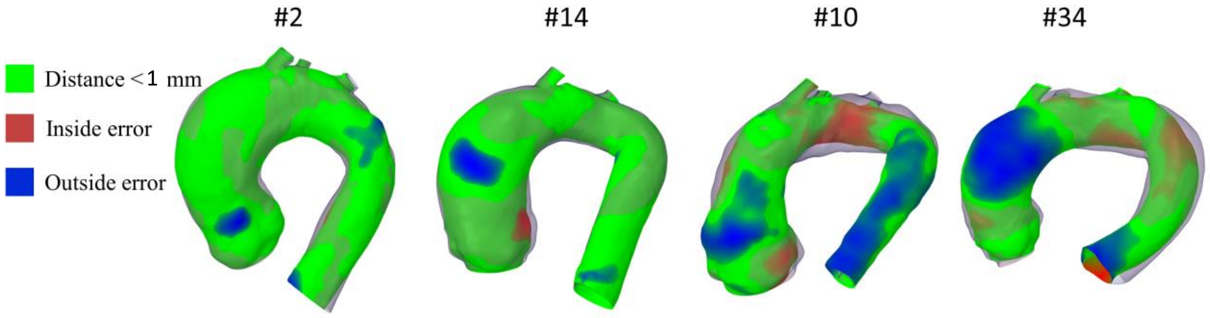

Leave-one-patient-out validation results

Shape reconstruction by least squares fitting

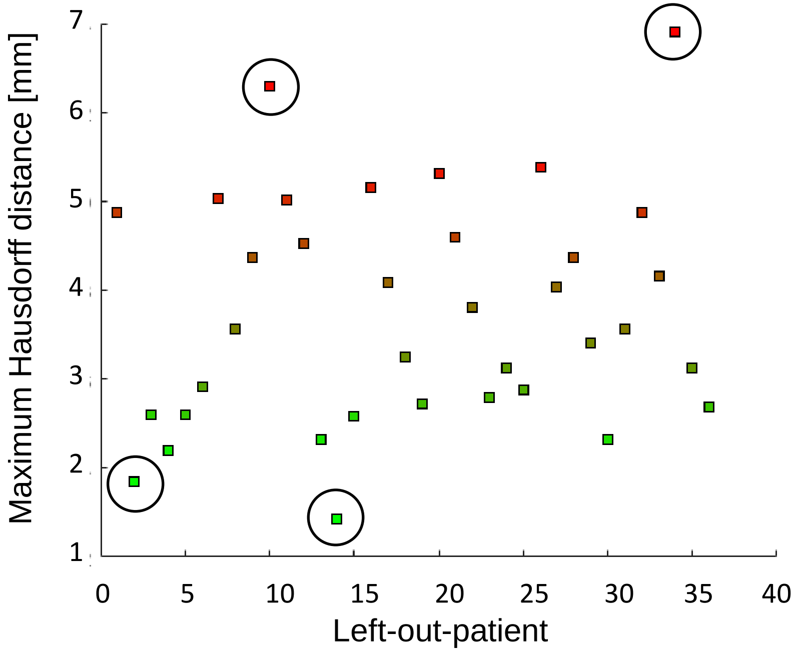

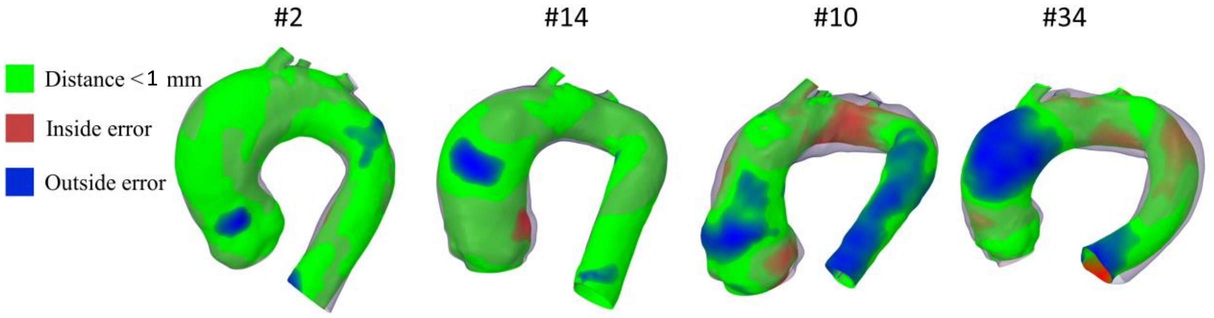

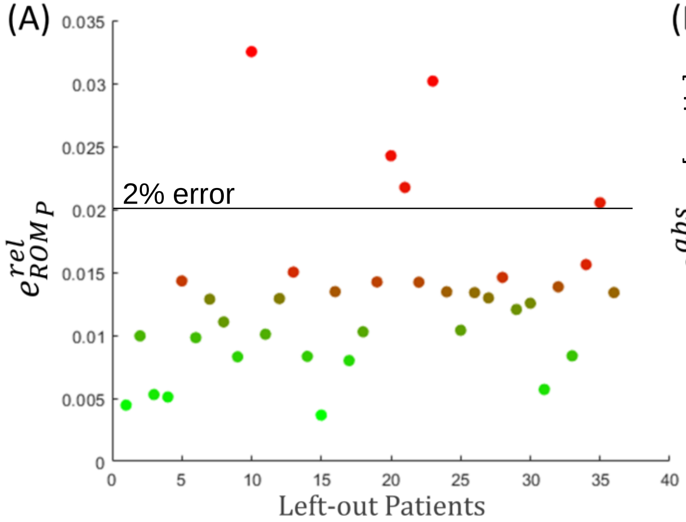

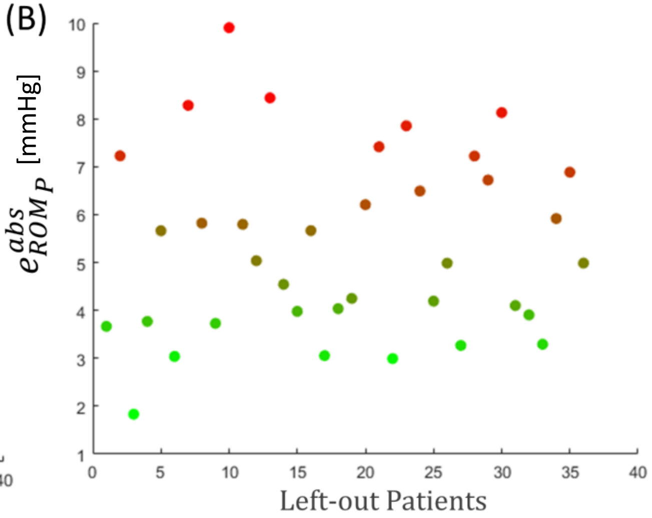

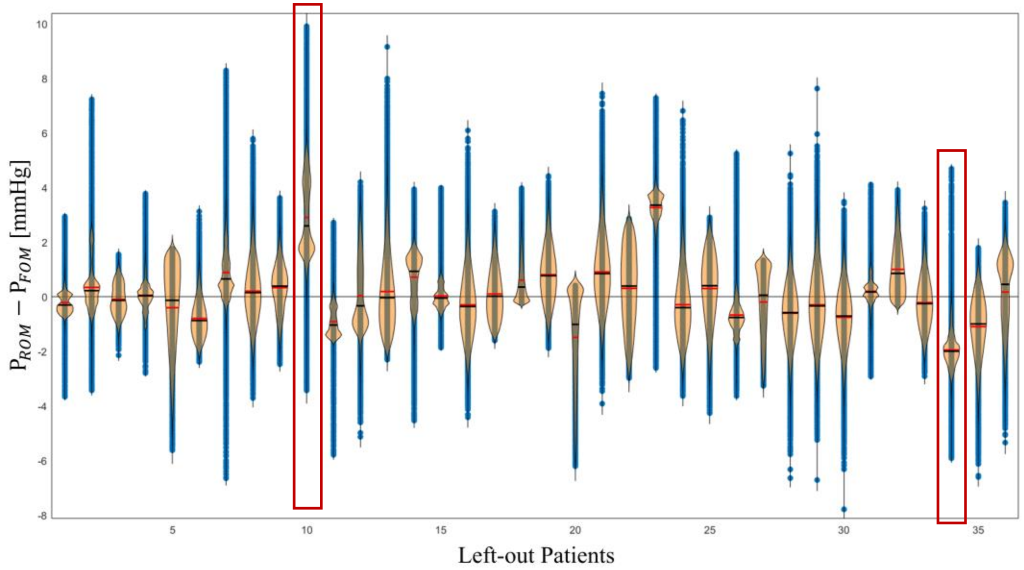

Leave-one-patient-out validation results

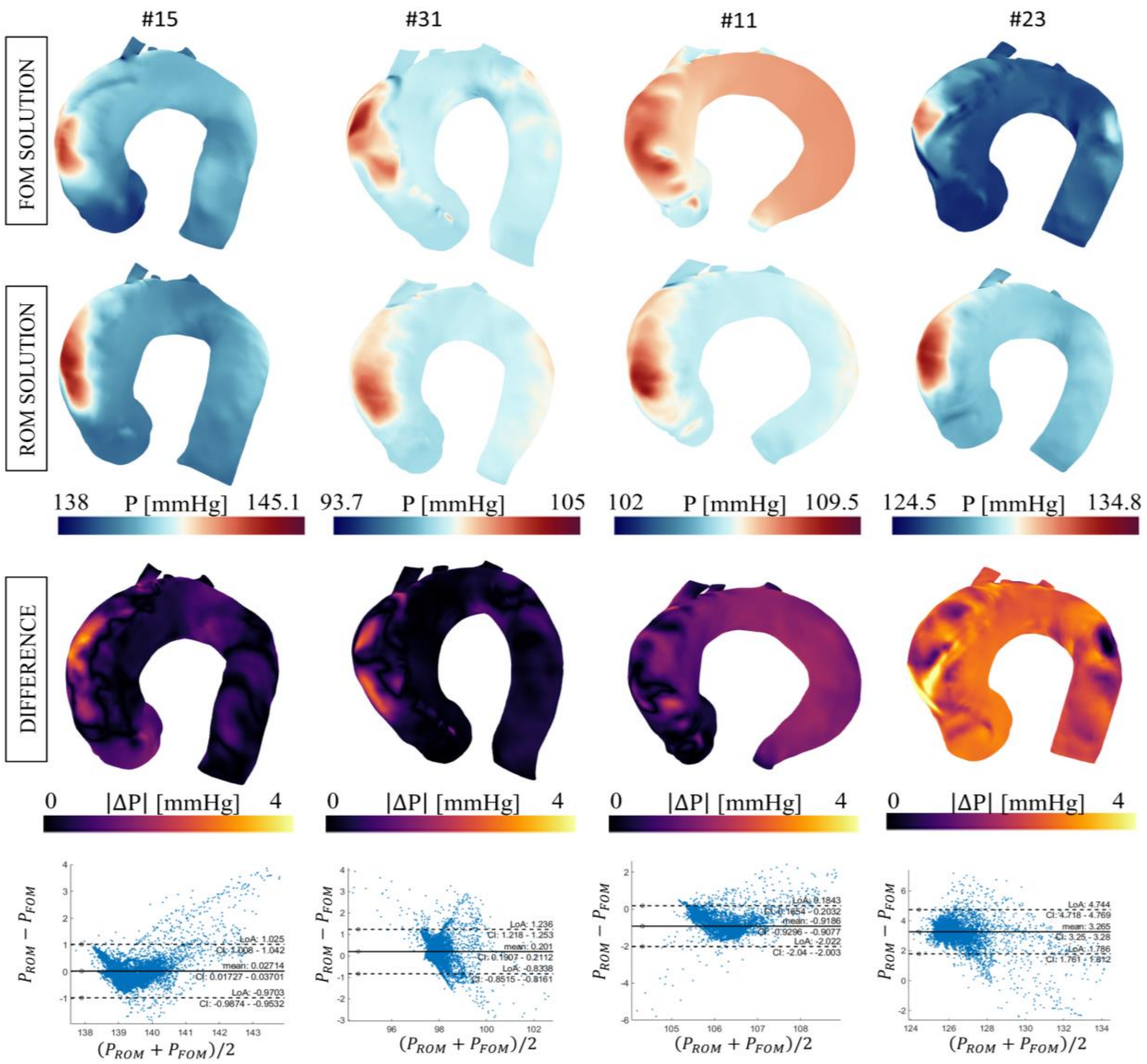

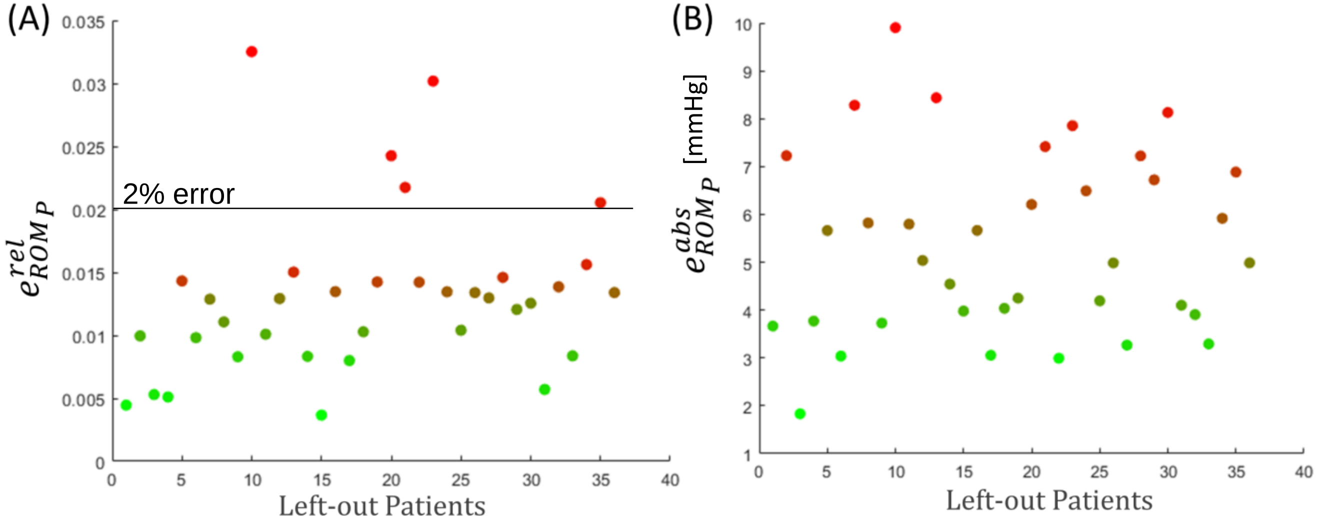

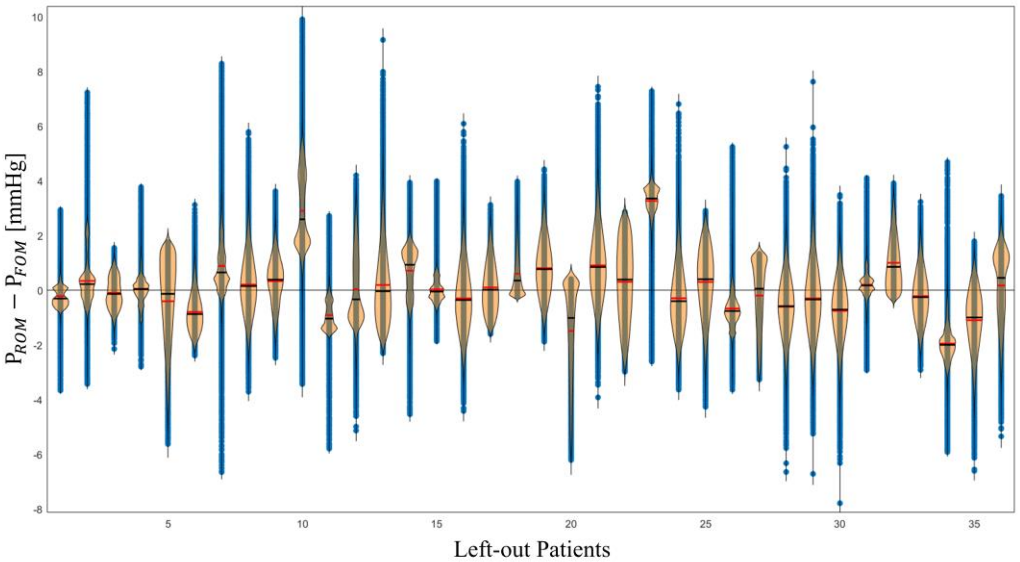

Discussion

- **Mathematical, statistical and numerical** techniques can be combined to **predict** in almost real-time **hemodynamic results** directly starting from the medical images.

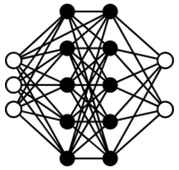

- Patients for whom the reconstruction is outside the modal space used to train the ROM return higher errors in predicting the output wall pressure field.

MAIN LIMITATIONS

- A small set (35) of patients is used to compute the statistical shape model.

- A validation of the hemodynamic results needs to be performed.

Conclusions

With this work, we analysed some of the **fundamental aspects** for the **construction** of a **Digital Twin**.

The basis of a reliable Digital Twin must be **clean and accurate data**

A Digital Twin requires **dynamic integration** of patient data through computational and statistical models

The Digital Twin must integrate both **anatomical** and **physiological** data to understand the disease progression

A Digital Twin based on high-fidelity data should be able to accurately predict the disease **risk**

Conclusions

LIMITATIONS AND FUTURE WORKS

All the **separately analyzed** parts should be **integrated** to create a real active Digital Twin

The Digital Twin needs to be made **more accessible for medical personnel**

The methods proposed here need to be extended on a **larger scale**

Wearable device integration will enable more responsive updates based on patients’ condition

List of Publications

- **Geronzi, L.**, et al. (2021). High fidelity fluid-structure interaction by radial basis functions mesh adaption of moving walls: a workflow applied to an aortic valve. *Journal of Computational Science*, *51*, 101327 (*published*).

- **Geronzi, L.**, et al. (2023). "Assessment of shape-based features ability to predict the ascending aortic aneurysm growth." Frontiers in Physiology 14: 378. (*published*).

- **Geronzi, L.**, et al. (2023). "Computer-aided shape features extraction and regression models for predicting the ascending aortic aneurysm growth rate." Computers in Biology and Medicine 162: 107052 (*published*).

- **Geronzi, L.**, et al. (2023). "Calibration of the mechanical boundary conditions for a patient-specific thoracic aorta model including the heart motion effect." IEEE Transactions on Biomedical Engineering (*published*).

- **Geronzi, L., et al.** (2023). "A Parametric 3D Model Of Human Airways For Particle Drug Delivery And Deposition." Fluids (*submitted*)

- Marin-Castrillon, D.M., **Geronzi, L.**, et al. (2023). "Segmentation of the aorta in systolic phase from 4D flow MRI: multi-atlas vs. deep learning." Magnetic Resonance Materials in Physics, Biology and Medicine: 1-14 (*published*).

- Martínez, A., Hoeijmakers, M., **Geronzi, L.**, et al. (2023). "Effect of turbulence and viscosity models on wall shear stress derived biomarkers for aorta simulations." *Computers in Biology and Medicine*, 107603 (*published*).

- Emendi, M., Karampiki, E., Støverud, K., Martinez, A., Geronzi, L., (2023). "Towards a Reduced Order Model for EVAR Planning and Intra-operative Navigation", Medical Engineering & Physics (*under review*)

THANK YOU FOR THE ATTENTION

TOR VERGATA
UNIVERSITÀ DEGLI STUDI DI ROMA